**Ismail M, Liu W, Chan MSC, Dunstan MT, Scott SA. Synthesis, Application, and Carbonation Behavior of $Ca_2Fe_2O_5$ for Chemical Looping $H_2$ Production.**
***Energy & Fuels* 2016, 30(8), 6220-6232.**

# Synthesis, Application and Carbonation Behaviour of $Ca_2Fe_2O_5$ for Chemical Looping $H_2$ Production

*Mohammad Ismail[1]*, Wen Liu[2], Martin S. C. Chan[3], Matthew T. Dunstan[4] and Stuart A. Scott[1]*

*[1]Department of Engineering, University of Cambridge, Cambridge, CB2 1PZ, UK.*
*[2]Cambridge Centre for Advanced Research in Energy Efficiency in Singapore, Nanyang Technological University, Singapore 138602*
*[3]Department of Chemical Engineering & Biotechnology, University of Cambridge, Cambridge, CB2 3RA, UK.*
*[4]Department of Chemistry, University of Cambridge, Cambridge, CB2 1EW, UK.*

## Abstract

Chemical looping hydrogen production uses the oxidation and reduction of metal oxides, typically iron, to produce hydrogen. This work focuses on the modification of iron oxide with calcium oxide to form an oxygen carrier containing di-calcium ferrite ($Ca_2Fe_2O_5$), which presents favourable thermodynamics for achieving higher conversions of steam to hydrogen compared to chemically unmodified iron oxide. Different methods of synthesis, *viz.* mechanochemical synthesis and co-precipitation, were used to produce $Ca_2Fe_2O_5$, and their resulting performances were compared. Consistent with thermodynamic predictions, it was found that $CO_2$, or steam, was sufficient to fully regenerate the reduced carriers to $Ca_2Fe_2O_5$. The cyclic stability of the oxygen carriers were studied in fluidised bed reactors and by thermogravimetric analysis (TGA). Good stability of the materials was observed for up to 50 cycles, with no evidence of agglomeration even up to 950 $^oC$. The rate of deactivation was found to correlate with the purity of $Ca_2Fe_2O_5$ and the presence of impurity phases such as $CaFe_2O_4$, which tended to segregate into its constituent elemental oxides. Carbonation of the oxygen carriers was examined by TGA, and was found to occur appreciably only for the reduced carrier (a mixture of CaO and Fe) between temperatures of 500 – 700 $^oC$ and 0.1 – 0.5 atm of $CO_2$, whereas the oxidised carrier (*viz.* $Ca_2Fe_2O_5$) did not carbonate. Fresh and cycled materials were characterised by XRD, SEM and BET analysis. $Ca_2Fe_2O_5$ is a potentially viable material as an oxygen carrier for hydrogen production, but owing to thermodynamic limitations cannot be used for complete fuel oxidation.

**Keywords:** Chemical Looping Hydrogen Production; Carbon Dioxide Capture; Fluidised Bed; Di-calcium Ferrite; Carbonation Reaction.

*** Corresponding author:**
*Energy laboratory, ISO-45, Department of Engineering*
*University of Cambridge, Trumpington Street, Cambridge, CB2 1PZ, United Kingdom*
*Phone: +447841419325, Fax: +441223765311, E-mail: mi286@cam.ac.uk*

## 1. Introduction

The combustion of fossil fuels *e.g.* coal or gas for electricity generation, is a major contributor (~ 43%) of the total anthropogenic emission of $CO_2$.[1] Carbon capture and storage (CCS) is a potential scheme for capturing $CO_2$ from fossil fuel combustion.[2,3] The objective of carbon capture is to produce a relatively pure stream of $CO_2$, free from nitrogen. Proposed strategies for CCS *e.g.* post-combustion capture, pre-combustion capture, and oxy-fuel combustion are associated with significant energy penalties [2]. One such strategy, chemical looping combustion (CLC), combusts fossil fuels using redox cycles of oxygen carriers (typically transition metal oxides) whilst producing a pure stream $CO_2$ suitable for sequestration.[4] For CLC, where the focus has been on reducing the cost per ton of $CO_2$ sequestered, the cost of replacing the degraded oxygen carrier has been a concern, leading to the suggestion that low cost minerals *e.g.* ilmenite ($FeTiO_3$) should be used.[5]

The chemical looping approach can also be used for hydrogen production in a process known as the 'cyclic-water gas shift' or the 'steam-iron' process.[6,7,8,9,10] In the steam-iron process, the oxygen carrier is oxidised by steam to produce hydrogen; the process can also be modified to produce sequesterable $CO_2$ by fully reoxidising the carrier in air, and ensuring that the fuel is brought to equilibrium with the fully oxidised carrier.[11,12] Thus, chemical looping hydrogen production (CLHP) could be achieved using an extra reactor,[11] packed beds operating transiently[6,13] or a counter current moving bed.[14,15] Oxides of iron are suitable oxygen carriers as they show multiple phase transitions with different oxidising potentials (*viz.* the equilibrium fugacity of oxygen) that are each suitable for either complete combustion or hydrogen production.[16] For example, the $Fe_2O_3 \rightarrow Fe_3O_4$ transition allows for nearly complete combustion, whilst $Fe_3O_4 \rightarrow FeO$ and $FeO \rightarrow Fe$ transitions have very low equilibrium oxygen fugacities. The later transitions cannot be used for full combustion of fuel, but can be used for splitting water to produce $H_2$. Using chemical looping processes for $H_2$ production, can also lead, at least in theory, to more efficient production; for example, using the $FeO \rightleftharpoons Fe_3O_4$ transition in a cyclic water gas shift process can result in exergy losses which are ¼ of those seen in a traditional water gas shift process.[10]

Materials used for chemical looping combustion and hydrogen production (CLCHP) need to have sufficient physical strength, oxygen-carrying capacity, reactivity and stable performance over many redox cycles[17] and should be cost effective and environmental friendly. Since unsupported $Fe_2O_3$ suffers from agglomeration, sintering and activity loss, especially when reduced to metallic Fe at high temperatures,[6,18,19] various inert supporting materials, *e.g.* oxides of Mg,[20] Al,[21,22] Ca,[23] have been mixed with iron oxide to improve its properties.

Improved performances were also reported for materials consisting of two or more active metal oxides.[24,25,26,27] $NiFe_2O_4$ and $CoFe_2O_4$ have also been suggested as possible materials for hydrogen production.[7,25]

CaO is a potential support for iron oxide in consideration of stability,[23] availability, as well as cost, and was found to compare favourably with MgO, $TiO_2$, $Al_2O_3$.[28] The cost of producing manufactured oxygen carriers (compared with using low cost minerals) will be an important consideration in the economics of chemical looping hydrogen production. Both iron and calcium are relatively cheap raw materials, and the cost of processing could be offset by both increases in reactivity compared with minerals, changes to the thermochemistry that enable process improvements, and minimising the rate of replacement of the oxygen carrier by using materials which lower rates of degradation. In addition, spent iron oxide contaminated with calcium oxide, poses little environmental hazard, and could potentially be recycled, *e.g.* in a steal making process.

From the thermodynamics of the Ca-Fe-O system,[29,30] it can be seen that addition of CaO to $Fe_2O_3$ can form various ferrite phases, for example, mixing of 66.7 mol.% CaO with 33.3 mol% $Fe_2O_3$ at ~ 700 – 1445 ºC in air produces di-calcium ferrite ($Ca_2Fe_2O_5$, denoted here as $C_2F$). The brownmillerite structured $C_2F$ consists of alternating octahedral (type A) and tetrahedral (type B) layers and is effectively an anion-deficient perovskite with ordered oxygen vacancies, [31,32] which displays high ionic conductivity.[33] In addition, $C_2F$ contains superoxide radicals ($O_2^-$) on the surface and $Fe^{4+}$ at temperatures lower than those used for CLC,[34,35] making it a good catalyst for the oxidation of CO and $NH_3$,[36] and for the gasification of biomass.[37,38] Other perovskites have found to use in chemical looping as active oxygen carriers[25] and supports,[39] to improve activity and cyclic stability.[40] Pure $C_2F$ cannot easily be formed by the simple mechanical mixing of CaO and $Fe_2O_3$.[31] In fact, the purity of the $C_2F$ depends on a variety of factors including the preparation method, [31,34,41,42] the nature of the raw materials[43] and the subsequent thermal treatment.[31]

The performance of $Fe_2O_3$-based oxygen carriers containing lower amount calcium,[23] and mixed ferrite phases[44] has previously been reported. The mixture of phases seemed to result in improved cyclic stability, but the formation of $C_2F$ rather than the mono-calcium ferrite ($CaFe_2O_4$, denoted here as CF) reduced the oxygen-carrying capacity for complete combustion. The reduction pathway was also complicated by the formation of different ferrites as oxygen was removed from the material. As discussed below, the phase diagram for this system, suggests that whilst the $C_2F$ phase hinders full combustion, the material may be suitable for use in a hydrogen production process. The objective of this study is to develop oxygen carriers

consisting of pure $C_2F$ and to investigate the performance of the synthesised $C_2F$ for hydrogen production. The interaction between the $Fe_2O_3$ and CaO during the cyclic redox process is also examined.

## 2. Thermodynamics

The thermodynamics of Fe-Ca-O system are well known and is demonstrated by the phase diagram shown in Figure 1. $C_2F$ should only undergo a single redox reaction ($Ca_2Fe_2O_5 \rightleftharpoons 2CaO + 2Fe + 1.5O_2$)[30,45,46] without any intermediate phase transitions[47] in contrast to CF which undergoes multiple redox reactions. Figure 1 shows the equilibrium partial pressure of oxygen, obtained from (a) MTDATA using the NPL Oxide Database[46] and (b) calculated from the reported free energies of the following reactions:

$$2CaO_{(s)} + Fe_2O_{3(s)} \rightleftharpoons Ca_2Fe_2O_{5(s)}^{45,48,49} \quad (1)$$

$$2Fe_{(s)} + 1.5O_{2(g)} \rightleftharpoons Fe_2O_{3(s)}^{50} \quad (2)$$

The two data sources shown in Figure 1 agree reasonably well with each other and show that very low oxidising potentials (*viz.* strongly reducing atmospheres) are needed to reduce $C_2F$ to CaO and Fe. While this means that the reduction of $C_2F$ to CaO and Fe could not be used to achieve complete combustion, this redox transition can readily produce $H_2$ by oxidation with steam (with a higher equilibrium ratio of steam: hydrogen than if pure iron oxide is used).

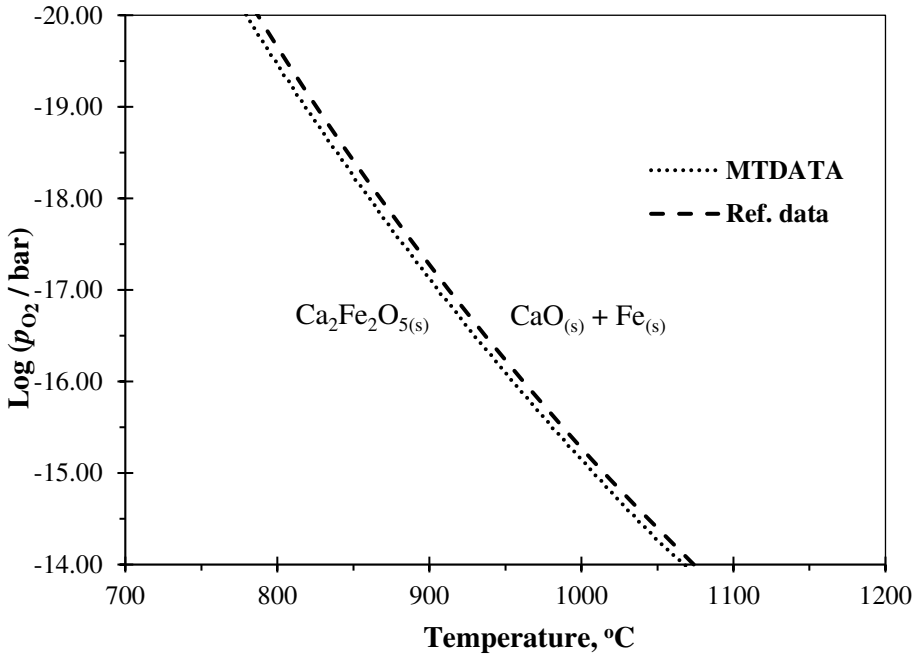


*Figure 1: $P_{O_2}$ - T phase diagram of the Ca-Fe-O system obtained using MTDATA[46] and reported reference data.*[45,48,49,50]

In any fuel combustion process, there is likely to be a high background concentration of $CO_2$, therefore carbonation also needs to be considered. Figure 2 shows the regions of stability

of the ferrite and carbonate phases in different $CO_2$ atmospheres, assuming the following reactions:

$$Ca_2Fe_2O_{5(s)} + 2CO_{2(g)} \rightleftharpoons 2CaCO_{3(s)} + Fe_2O_{3(s)} \quad (3)$$

$$CaFe_2O_{4(s)} + CO_{2(g)} \rightleftharpoons CaCO_{3(s)} + Fe_2O_{3(s)} \quad (4)$$

where $P_{CO_2}/(1\ \text{bar}) = \exp(-\Delta G^o/RT)$ at equilibrium, with $\Delta G^o$ calculated from the free energy of formation of $C_2F$, CF[45,48] and $CaCO_3$.[51] When the partial pressure of $CO_2$ is greater than the equilibrium value at a given temperature, the material may carbonate and produce $Fe_2O_3$. Thus, thermodynamically, both the CF and $C_2F$ phases are more stable and more difficult to carbonate than CaO, with calcium ferrite only able to carbonate at lower temperatures. $C_2F$ and CF would not be expected to carbonate at temperatures typically used for chemical looping, *i.e.* $T$ > 850 °C. However, during the reduction stage of CLCHP, $C_2F$ reduces to Fe and CaO, which could potentially carbonate.

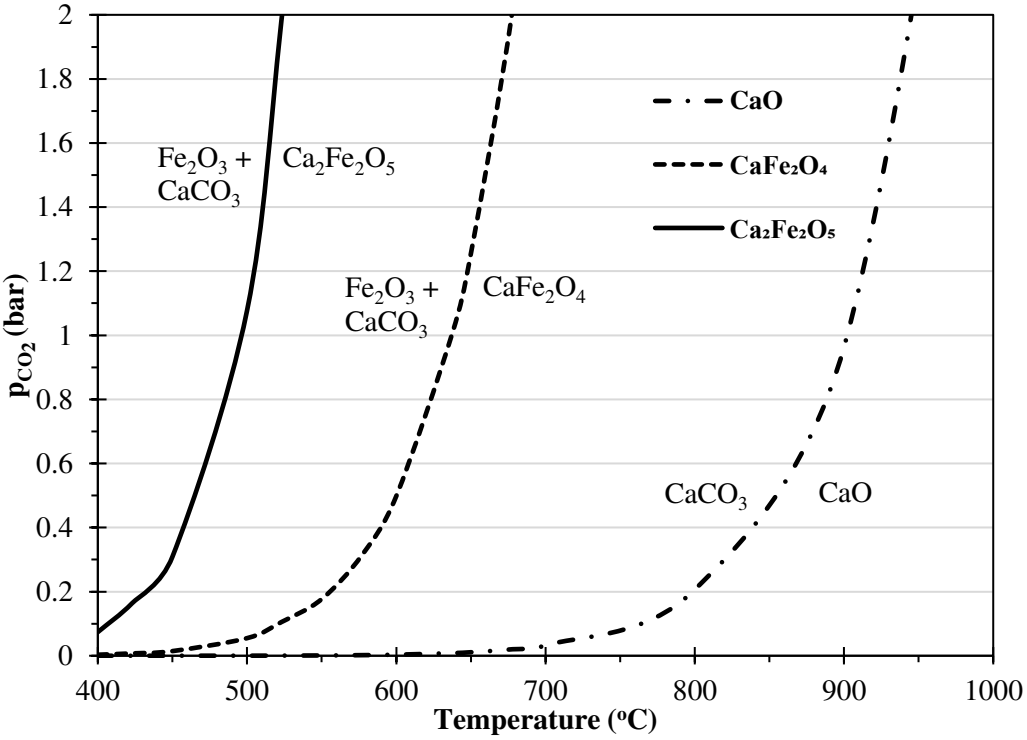


*Figure 2: Equilibrium partial pressure of $CO_2$ for the CaO - $CO_2$, $CaFe_2O_4$ - $CO_2$ and $Ca_2Fe_2O_5$ - $CO_2$ systems as a function of temperature using different reference data.*[45,48,49,51]

## 3. Experimental

### 3.1 Material Preparation

**Wet-granulation:** Unsupported iron oxide (named FC0) particles were prepared by spraying water onto iron oxide powders (99%, Sigma-Aldrich, $d_p$ < 5μm). The mixture was

stirred simultaneously and the resulting agglomerates were sieved to obtain particles in the size range 425 – 500 μm. The raw particles were then sintered at 1000 $^{o}$C for 6 h in air and re-sieved to ensure particles of the desired size range.

The particles containing 66.7 mol% CaO and 33.3 mol% $Fe_2O_3$ (named as 'FC67') were made using two different methods, outlined below:

**Mechanochemical Synthesis (MCS) Method:**

A powdered mixture consisting of required amount of CaO (97+%, Acros Organics, calcined at 1000 $^{o}$C for 10 mins in a furnace to decompose any carbonates or hydroxides) and $Fe_2O_3$ was mixed with a small amount of ethanol (99.8+%, Fisher Scientific) to aid mixing, and ball milled (SFM-1, MTI Corporation) for 3 h at 1800 rpm. The milled slurry was calcined at 1000 $^{o}$C – 1250 $^{o}$C for 6 – 36 h, depending on the sample, and then crushed and sieved to recover 425 – 500 μm particles.

**Co-precipitation (COP) Method:**

Separate aqueous solutions of 1M $Fe(NO_3)_3 \cdot 9H_2O$ and 1M $(Ca(NO_3)_2.4H_2O$ were mixed to give a ratio of Fe:Ca equivalent to 66.7 mol.% CaO and 33.3 mol.% $Fe_2O_3$. The pH of the solution was raised by adding various alkaline precipitants: 1M $NH_4OH$, 1M $(NH_4)_2CO_3$ + 1 M $NH_4OH$ (50:50, v/v), 1M NaOH, or a mixture of 1 M of NaOH + 1 M of $Na_2CO_3$ (50:50, v/v). The precipitant was added drop-wise to the vigorously stirred, $N_2$-blanketed, aqueous solution until the pH (measured using a Jenway 3540 pH/conductivity meter) of the solution reached the desired value of 10 or 12.5. In the case of addition of 1M $(NH_4)_2CO_3$ + 1M $NH_4OH$ (50:50, v/v), the maximum pH of the slurry obtained was 8.5, hence, to obtain the desired pH, additional 1M $NH_4OH$ was added. All the slurries were aged for 6 h. The slurry prepared using NaOH or $NH_4OH$ was aged under a $N_2$-blanket to minimise the contamination by atmospheric $CO_2$. The precipitates were then filtered, washed with DI water for 3 – 4 times, dried at ~ 80 $^{o}$C for 24 h, calcined at 1000 $^{o}$C – 1250 $^{o}$C for 6 – 12 h, depending on the sample, and then crushed and sieved to 425 – 500 μm particles.

### 3.2 Thermogravimetric analysis of the oxygen carriers

Redox cycles, temperature programmed reduction (TPR) and carbonation were performed in a thermogravimetric analyser (Mettler Toledo TGA/DSC-1). A permanent flow of $N_2$ (zero grade, BOC) was used as the protective gas and purge gas (both flowing at 50 mL/min, as measured at 20 $^{o}$C and 1 atm) in all experiments. All of the gases used were BOC standard grade and in all cases, a flow rate of 50 mL/min was maintained. Between each reduction and oxidation stage, the reactive gas line was purged with $N_2$ for 2 mins.

In a typical CLC cycling experiment, 25 to 30 mg of the oxygen carrier particles were heated to 900 °C at a rate of 20 °C/min with air as the reactive gas. The oxygen carrier was then exposed to alternating reducing and oxidising environments for up to 50 redox cycles. In a TPR experiment, 25 to 30 mg of the oxygen carrier was placed in a 70 µL alumina crucible, and subjected to the following conditions: (i) degassing by heating to 1000 °C at 20 °C/min, holding for 10 mins and cooling to 200 °C at −10 °C/min in air, (ii) reduction by holding for 10 mins at 200 °C, heating to 1050 °C at a rate of 5 °C/min then holding for 2 – 3 h in 5 vol.% $H_2$ in $N_2$. In a carbonation experiment, $CO_2$ was used in place of the 5 vol.% $H_2$.

The changes in conversion of the metal oxide during the oxidation ( $\Delta X'_{ox}$ ) and reduction ( $\Delta X'_{red}$ ) stages within a cycle in a redox experiment were calculated from

$$\Delta X'_{red} = (m_0 - m) / \Delta m_{\max} \quad (5)$$

$$\Delta X'_{ox} = (m - m_0) / \Delta m_{\max} \quad (6)$$

where $m$ is the mass of sample, $m_o$ is the initial mass of the sample at the start of the stage within a cycle and $\Delta m_{\max}$ is the mass change expected if all of the $Fe^{3+}$ in the sample is reduced to metallic Fe. The changes in conversion, $\Delta X'_{ox}$ and $\Delta X'_{red}$, then give a measure of the oxygen transferred during a cycle.

### 3.3 Cyclic Performance of Oxygen Carriers in Fluidised Bed Reactors

Two different fluidised bed reactors, 'FBR-1' and 'FBR-2', were used to study the performance of the oxygen carriers. FBR-1[44] and FBR-2[52] are described elsewhere. In FBR-1, $CO_2$ was used as the oxidant during the re-oxidation of the reduced oxygen carrier (producing CO) whilst, in FBR-2, steam was used as the oxidant (producing $H_2$). Using $CO_2$ as the oxidant in FBR-1 avoided the complications with the feeding of steam and subsequent gas analysis, and the conversion of Fe and FeO to $Fe_3O_4$ with $CO_2$ is thermodynamically similar to oxidation with steam at 850 °C (the equilibrium constant for the water-gas shift reaction is close to unity at this temperature).[27]

The reactor of FBR-1 was made of recrystallized $Al_2O_3$ (Almath Crucibles Ltd.), with an i.d. of 19.5 mm and a length of 676 mm. The reactor of FBR-2 consisted of an electrically heated tube (Incoloy 800 HT) with an i.d. of 16 mm and a length of ~140 mm. During a typical experiment, ~10 mL and ~ 4 mL bed of recrystallised $Al_2O_3$ sand ($d_p$ ~ 400 µm) were introduced in the reactors of FBR-1 and FBR-2, respectively, as bed material. The bed was then electrically heated to the required temperature, while being fluidised by $N_2$ at a flow rate 1.8 L/min (at 20 °C and 1 atm). At the set-point temperature, 0.5 g of oxygen carrier was then added to the hot

bed in each of the reactors. The nominal flowrate of the fluidising gas was maintained at 1.8 L/min (as measured at 20 °C and 1 atm), which corresponds to a $U/U_{mf}$, ≈ 7.0 (in FBR-1) and 10.5 (in FBR-2), where $U$ is the superficial velocity of the fluidising gas and $U_{mf}$ is the minimum fluidisation velocity (calculated using Wen and Yu's correlation [53]). The effluent gas was sampled, at a rate of 0.5 L/min, and dried in a tube packed with $CaCl_2$ pellets, before being analysed in a non-dispersive infrared (NDIR) gas analyser (Uras26, EL3020, ABB), which measures [CO] and [$CO_2$]. In the case of FBR-2, an additional condenser immersed in an ice bath was fitted upstream of the $CaCl_2$ pellets, and a thermal conductivity analyser (Caldos27, EL3020, ABB) was also used (installed in parallel to the NDIR gas analyser) to measure the concentration of $H_2$. At the conclusion of the experiment, the solid samples were recovered from the hot reactor rapidly under suction and cooled under a flow of 2.0 L/min of $N_2$.

Table 1 summarises the experimental conditions used during the cycling experiments. Between each stage, the reactors were purged with $N_2$ for 2 mins in FBR-1 and 1 min in FBR-2.

*Table 1: Feed compositions, duration, and temperature in different experiments in FBR-1 and FBR-2.*

| **Reactor** | **Reducing gas** | **Time (min)** | **Oxidizing gas** | **Time (min)** | **Air ox. time (min)** | **Temp. (°C)** |
|---|---|---|---|---|---|---|
| FBR-1 | 10 vol% CO | 3 | 20 vol% $CO_2$ | 3 | 3 | 850 |
| FBR-1 | 10 vol% CO | 13 | 20 vol% $CO_2$ | 13 | 8 | 850 – 950 |
| FBR-1 | 10 vol% CO | 20 | 20 vol% $CO_2$ | 12 | 8 | 900 |
| FBR-2 | 10 vol% CO | 13 | ~8 vol% steam | 13 | 8 | 900 |

The moles of $CO_2$ produced during reduction by CO, $N_{CO_2}$, and that of CO produced during oxidation by $CO_2$, $N_{CO}$, were calculated from the measured mole fractions in the off-gas, $y_{CO_2}$, $y_{CO}$ and the total molar flow $\dot{N}_T$ using $N_{CO_2} = \dot{N}_T \times \int y_{CO_2} dt$ and $N_{CO} = \dot{N}_T \times \int y_{CO} dt$, respectively. The change in conversion during reduction, $\Delta X_{red}$, was calculated using $\Delta X_{red} = 1000 \times N_{CO_2} / (18.75 \times 0.5 \times x_{Fe_2O_3})$, whereas the change in oxidation conversion, $\Delta X_{ox}$, (equivalent to Fe to $Fe_3O_4$ conversion) was calculated as $\Delta X_{ox} = 1000 \times N_{CO} / (16.67 \times 0.5 \times x_{Fe_2O_3})$; here $x_{Fe_2O_3}$ is the mass fraction of $Fe_2O_3$ in the sample. The constants 18.75 and 16.67 are the theoretical amounts of oxygen atoms that could be transferred if fully reduced $Fe_2O_3$ was oxidized to hematite and magnetite, respectively (in mmol of 'O' per gram of $Fe_2O_3$).

This later definition of change in conversion during oxidation (in the case of FBR) differs slightly from that used in the TGA experiments ( $\Delta X'_{ox}$ ) owing to it being normalised by the amount of oxygen transferred if the fully reduced material were to be fully reoxdised from metallic Fe to an oxidation state equivalent to magnetite (as opposed to hematite, in the earlier definition).

The amount of $H_2$ produced during steam oxidation was calculated by $N_{\mathrm{H_2}} = \dot{N}_T \times \int \frac{y_{H_2}}{1-y_{H_2}} dt$ and the change in oxidation conversion during steam to $H_2$ production was determined by $\Delta X_{\mathrm{H_2}} = 1000 \times N_{\mathrm{H_2}} / (16.67 \times 0.5 \times x_{\mathrm{Fe_2O_3}})$ . It should be noted that for experiments at or above 850 °C, carbonation would not be expected during either reduction or oxidation with $CO_2$ (from Figure 2, CaO will only carbonate below ~ 800 ºC with 20 vol% $CO_2$ at atmospheric pressure).

### 3.4 Characterisation of Oxygen Carriers

Powder X-ray diffraction (XRD) patterns of the particles were measured in the 2θ = 10 - 70º range using an Empyrean PANalytical diffractometer with Cu Kα radiation. Analysis of the data was carried out using the PANalytical X'Pert High Score Plus software. The XRD patterns were further analysed by Rietveld refinement using GSAS with the graphical interface EXPGUI[54,55] to identify the phase composition of the particles. Scanning electron microscopes (JEOL-5800LV and Zeiss EVO LS15) were used to study the surface morphology of the fresh and the reacted samples. For a cross-sectional view of the particles in the SEM, a conducto-mount (*i.e.* conductive Bakelite block) of the particles was prepared, and the cross-sections exposed by polishing. The BET surface area,[56] pore volume and pore diameters of the fresh and cycled materials were determined by $N_2$ adsorption at -196 ºC (TRISTAR 3000, Micromeritics).

## 4. Results

### 4.1 Parametric Study of FC67 ($C_2F$) Preparation Methods and Characterisation of the as-prepared Materials

#### 4.1.1 Co-precipitation Method and the Effects of the Choice of Precipitants

In the co-precipitation method, the control of pH, mixing, inclusion of contaminants *etc.* can influence the properties of the final oxygen carrier.[22,57,58] Here, the use of various precipitants and their effects on the fresh and cycled particles were investigated. The dried co-

precipitated particles (not calcined) contains mainly $Ca(OH)_2$, $Fe(OH)_3$ and some carbonates (when $Na_2CO_3$ or $(NH_4)_2CO_3$ was used as the precipitant)**, as shown in supporting documents Figure SI1.** The CaO and $Fe_2O_3$ (produced by the decomposition of nitrates, hydroxide carbonates *etc.*) should react with each other at the final calcination temperature to form only $C_2F$. However, a mixture of ferrite phases (CF and $C_2F$) was observed in the XRD patterns of the calcined particles **(shown in Figure SI2).**

During temperature programmed reduction (TPR), the particles prepared using $(NH_4)_2CO_3$, $Na_2CO_3$, $(NH_4)_2CO_3$ + $NH_4OH$ and $Na_2CO_3$ + NaOH as precipitants showed almost the expected mass loss upon complete reduction, whereas those prepared using NaOH (maintaining pH of 10 – 12.5) or $NH_4OH$ (pH of 10) showed a larger than expected mass loss (**shown in SI3**). The larger than expected mass loss implies some of the $Ca^{2+}$ remained in solution rather than precipitating out (owing to the high solubility product of $Ca(OH)_2$ *i.e.* $5.02\times10^{-6}$), even at moderately high pH.[59] This loss of CaO during precipitation (or during washing) can be avoided with the addition of $CO_3^{2-}$ ions. It is also worth mentioning that the poor mechanical strength of the particles produced using $(NH_4)_2CO_3$ or $Na_2CO_3$ as the sole precipitant or in combination with the equivalent hydroxide, particularly for particles made using $NH_4^+$ based precipitants.

### 4.1.2 Effect of Calcination Temperature and Duration

The temperature – composition phase diagram of the Ca-Fe-O system[29] shows that the CF is stable up to 1216 $^oC$, but forms slag at higher temperatures. Pure $C_2F$ is predicted to exist up to 1443 $^oC$. On cooling in air, after calcination, no phase transition is anticipated. The calcination temperature and duration for the dried (uncalcined) particles prepared by the COP and MCS methods were varied. Some materials were also re-calcined, to establish if the proportion of the $C_2F$ phase could be increased. Figure 3 shows the changes in the proportional amounts of each phase with increasing calcination duration, determined by Rietveld refinement of the XRD data (**presented in Figure SI4)** of the calcined particles prepared by MCS method. It can be seen that the relative abundance of $C_2F$ gradually increased with increasing calcination duration, with a corresponding decrease in the amount of CF and CaO. After 36 h of calcination at 1000 $^oC$, the material was mostly $C_2F$ (~ 86 wt.%) and CF (~14 wt.%), with no CaO detected. Therefore, it proved challenging to produce pure $C_2F$ using the solid state method, perhaps because of imperfect mixing between the CaO and $Fe_2O_3$, and slow solid state diffusion during calcination.

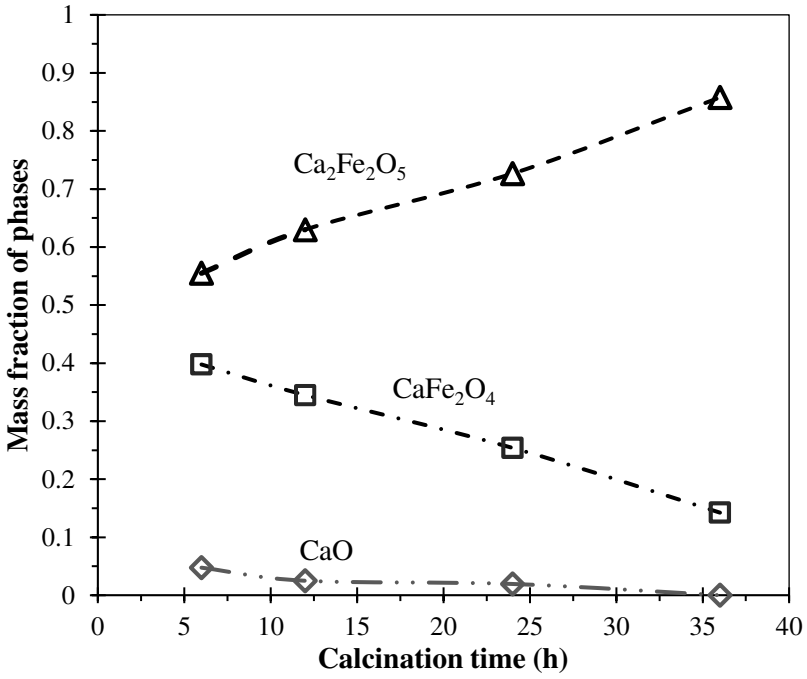


*Figure 3: Mass fractions of the crystalline phases (obtained from Rietveld refinements of the XRD patterns) present in FC67 prepared by MCS method in which the particles were calcined at 1000 °C for different time periods.*

Temperature programmed reduction (and their normalised rate of mass changes) of the materials (**shown in SI5**) showed two masses losses. The relative mass losses in the first and second stages of reduction give an indication of how much CF is present in the sample, the main impure phase. The first peak (*i.e.* the initial mass loss during TPR) is associated mainly with the reduction of CF to $C_2F$ (*i.e.* $CF \rightarrow 0.5C_2F + Fe + 0.75O_2$), which is consistent with previous work [44] suggesting that for mixtures containing CF and $C_2F$, CF first reduces to $C_2F$ before the $C_2F$ reduces.

A summary of the phase compositions obtained (i) by Rietveld refinement of the XRD patterns and (ii) from analysis of the initial mass loss in the TPR are shown **in Table SI1** for all materials tested. There is a strong correlation between the initial mass loss in TPR and the purity of the $C_2F$ obtained. A higher calcination temperature (>1000 °C) as well as a longer calcination duration promotes the formation of $C_2F$. However, the particles calcined at 1250 °C melted and were difficult to detach from the alumina crucible, meaning that the material could not be used for further experiments. Owing to the better dispersion of CaO and $Fe_2O_3$ in COP method, a near equilibrium phase composition was obtained by calcining for a shorter time compared to the MCS method. The iron content determined from Rietveld refinement analysis and TPR measurements was found to be very close to that required for pure $C_2F$.

## 4.2 Summary of Prepared Particles

For each of the synthesis methods, a selection of materials was further studied, as shown in Table 2, produced by: (2 - 3) MCS; (4) co-precipitation using $NH_4OH$ + $(NH_4)_2CO_3$; (5) co-precipitation using NaOH + $Na_2CO_3$. These materials will be referred to as FC67MCS, FC67(MCS,36h), FC67(COP,6h) and FC67(COP,12h), respectively. FC67MCS has a composition furthest from equilibrium and was selected as a contrast. FC0 (unmodified $Fe_2O_3$) was used as reference material.

*Table 2: Summary of the particles that are selected for further study*

| No. | Particles name | Calcination temperature | Weight fraction of $C_2F$[a] | Mole fraction of Fe in the material | | |
|---|---|---|---|---|---|---|
| | | | | Theoretically expected | XRD[a] | TPR[b] |
| 1 | FC0 | 1000 ºC, 6h | - | 1.0 | 1.0 | 1.0 |
| 2 | FC67MCS | 1000 ºC, 6h | 0.555 | 0.5 | 0.53 | 0.50 |
| 3 | FC67(MCS,36h) | 1000 ºC, 36h | 0.861 | 0.5 | 0.52 | 0.49 |
| 4 | FC67(COP,6h) | 1150 ºC, 6h | 0.919 | 0.5 | 0.47 | 0.51 |
| 5 | FC67(COP,12h) | 1000 ºC, 6h + 1150 ºC, 6h | 0.97 | 0.5 | 0.48 | 0.47 |

[a] Measured by Rietveld refinement of the XRD pattern.

[b] Measured by assuming the mass loss was solely due to the loss of oxygen from the reduction of Fe(III) to Fe(0).

## 4.3 Performance of Particles in Fluidised Bed Reactors: Effects of Temperature and the Extent of Reduction

Since FC0 was considered as the base material and all the modified oxygen carriers were compared with FC0, the times used for redox experiments were based on a preliminary observation that, within the selected timeframe, FC0 reduced to FeO and Fe. For example, FC0 showed a reduction conversion of 89.6 % after 13 minutes at 900 ºC in FBR-1, which means most of the $Fe_2O_3$ reduced to iron with some wüstite. A typical concentration profile observed during a cycling experiment in the fluidised bed is depicted in Figure 4, in this case for FC67MCS materials.

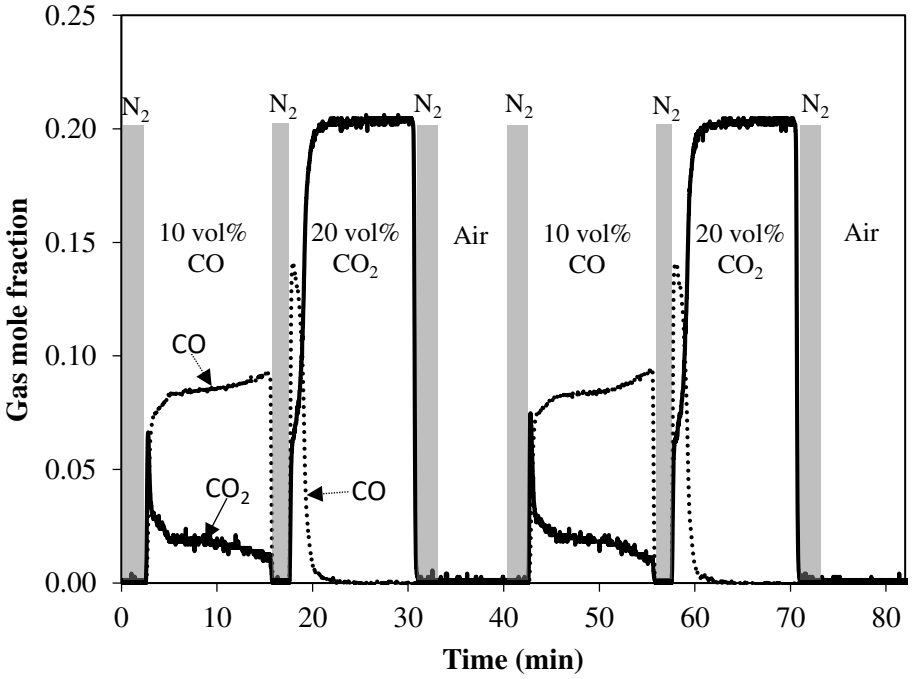


*Figure 4: Concentration profile of the off gases during the 1st and 2nd cycles in the cycling experiment of FC67MCS particles in FBR-1 at 850 °C.*

Figure 5a shows the amount of $CO_2$ produced during the reduction stage (for 13 mins) of cycling experiments of fresh particles in FBR-1 at different temperatures.

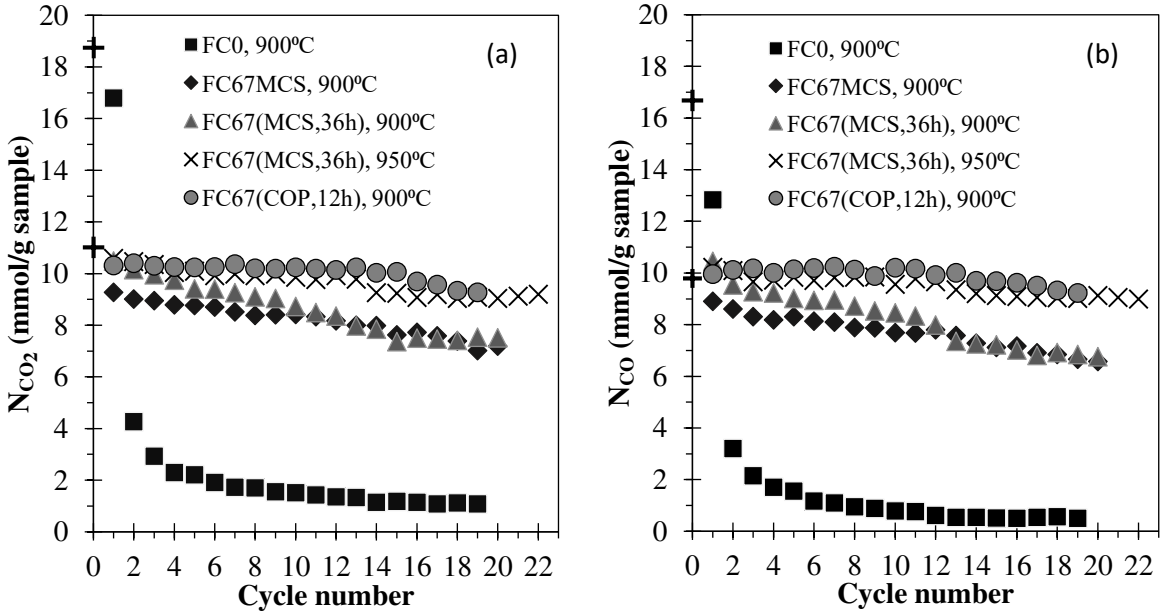


*Figure 5: Yield of (a) $CO_2$ during reduction with CO for 13 mins, (b) CO during oxidation with $CO_2$ for 13 mins in FBR-1 at 900 °C and at 950 °C. The '+' symbols on the Y-axis show in (a) the theoretically expected amount of $CO_2$ if FC0 and FC67 are reduced completely (18.75 mmol/g and 11.01 mmol/g, respectively) and in (b) the theoretically expected amount of CO if the completely reduced FC0 and FC67 are oxidised to a state equivalent to $Fe \rightarrow Fe_3O_4$ oxidation (16.67 mmol/g and 9.79 mmol/g, respectively).*

In Figure 5a, FC0 experienced a drastic loss in yield from the 2nd cycle onward. All the FC67 materials yielded less $CO_2$ per gram particles in the 1st cycle than for FC0, due to their lower specific iron content and lower reactivity. In the second and subsequent cycles, all the modified oxygen carriers produced more stable and higher yields of $CO_2$ than pure $Fe_2O_3$. Figure 5b shows that the yield of CO during oxidation with $CO_2$ at 900 °C follows a pattern similar to that seen in Figure 5a. Oxidation of reduced FC67 by $CO_2$ should produce 9.8 mmol CO /g if the carrier is oxidised back to a state equivalent to $Fe_3O_4$ (marked on Figure 7b), however the amount of CO exceeds this theoretical value for all the FC67 samples.

To study the stability of the oxygen carriers at various extents of reduction, the FC0 and FC67MCS samples were also tested for short and long redox cycling periods, maintaining the same reactive gases and flow rates. Figure 6 shows the amount of $CO_2$ produced when the oxygen carriers were reduced for 3 mins at 850 °C and 20 mins at 900 °C for up to 50 cycles.

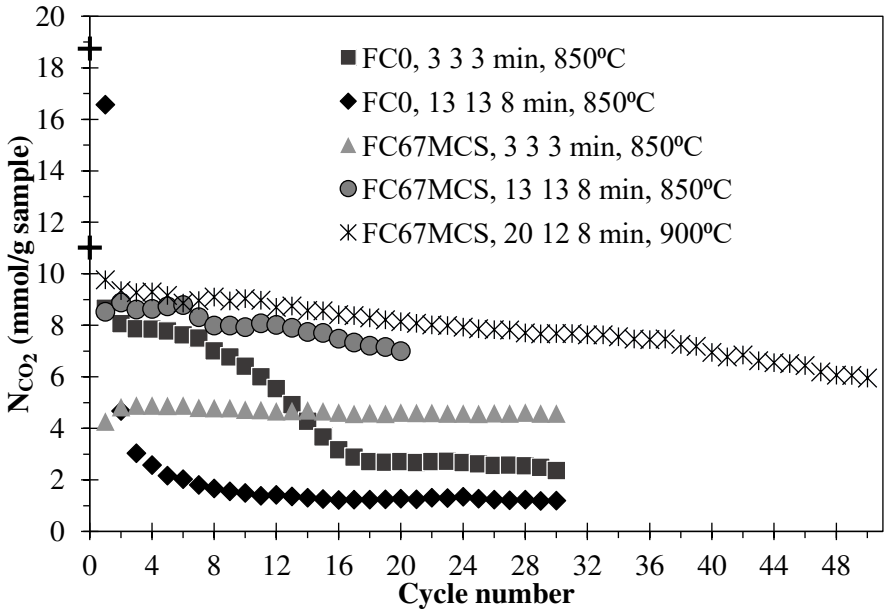


*Figure 6: $CO_2$ yield by FC0 and FC67MCS at different reaction temperatures and various reduction periods in FBR-1. The '+' symbols on the Y-axis show the expected amounts of $CO_2$ if FC0 and FC67 are reduced completely. The legend indicates the sample name, reduction & oxidation time and temperature. For example, 'FC0, 3 3 3 min, 850 °C' means FC0 particles were reduced for 3 mins with CO, partially oxidised for 3 min with $CO_2$ and then oxidised by air for 3 mins at 850 °C.*

Here, FC0 produced 8.7 mmol $CO_2$/g (46.2% conversion) in 3 mins in the 1st cycle at 850 °C, corresponding to the reduction to wüstite, with small amounts of Fe; subsequent yields rapidly decreased over successive cycles. For the longer cycles, the trend for FC0 at 850 °C follows a similar trend to that at 900 °C (shown in Figure 5). FC67MCS showed a stable yield of $CO_2$ (4.9 mmol/g, ~ 45% conversion) across the 30 cycles tested in 3 mins reduction at 850 °C. Upon increasing the reduction period to 20 mins and the temperature to 900 °C, the

same sample produced 9.8 mmol $CO_2$/g (~ 89% conversion) in the 1st cycle with a gradual degradation in yield in the following 50 cycles. This indicates that complete reduction of FC67MCS is difficult even with an increased temperature and reduction time.

To determine if comparable results would be obtained by oxidising in steam, rather than $CO_2$, a representative set of experiments were carried out using FBR-2. Figure 7 shows a comparison of the change in solid conversion of FC67(MCS,36h) during redox cycling experiments between FBR-1 and FBR-2 at 900 °C.

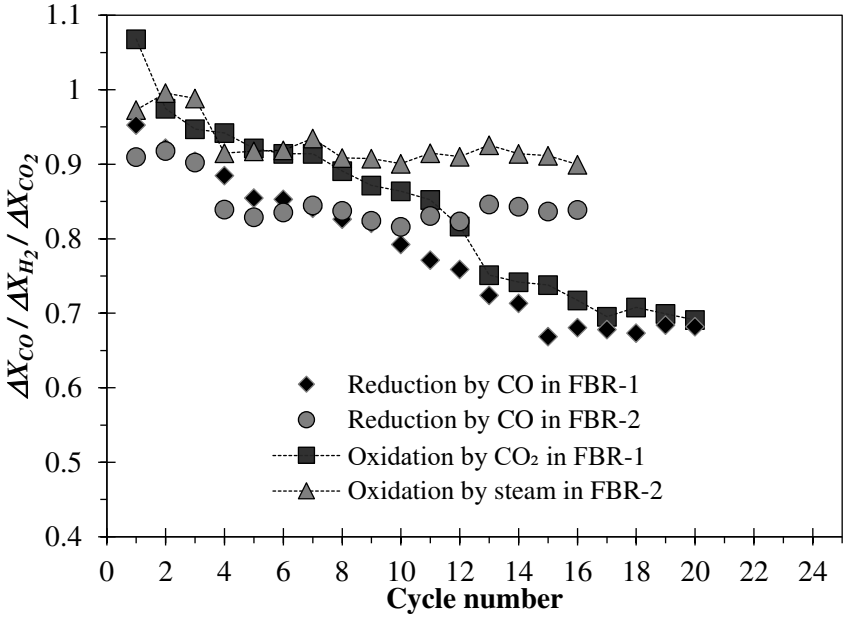


*Figure 7: Solid conversion (for the yield of $H_2$, CO or $CO_2$) versus cycle number of FC67(MCS,36h) oxygen carriers during redox cycles in FBR-1 and FBR-2 at 900 °C. A solid conversion of '1' means that all the iron species are fully reduced to Fe during reduction by CO or all the reduced Fe species are oxidised to $Fe_3O_4$ during oxidation by steam or $CO_2$.*

In both reactors, the reduction was for 13 mins, $CO_2$ (in FBR-1) or steam (in FBR-2) oxidation was for 13 mins and air oxidation was for 8 mins. A fluctuation in the $H_2$ yield during oxidation by steam was partially due to disturbances in the concentration and problems typically associated with feeding in steam (*e.g.* control of the saturator temperature). FC67(MCS,36h) showed an almost stable and a comparable performance in both systems, up to 11 cycles. After that, the oxygen carriers in FBR-1 showed a gradual decrease in conversion with increasing cycle number. It must be noted, that the reactors in the two systems (*i.e.* in FBR-1 and FBR-2) are of different sizes with different oxidants (10 vol.% $CO_2$ or ~8 vol.% steam) used for partial oxidation. The rate of reaction was not fully controlled by intrinsic kinetics, so the extent of reduction may have differed in a given cycle, which may have been the main cause of the observed differences between the two reactors. Nevertheless, it can be seen that the use of $CO_2$ as an analogue to steam produces qualitatively similar results.

### 4.4 Redox Cycles in TGA

Figure 8 shows the conversions achieved for different FC67 particles for up to 50 redox cycles at 900 ºC in the TGA. The particles containing a larger amount of $C_2F$ (*e.g.* FC67(MCS,36h) and FC67(COP,6h)), which is likely to be more difficult to reduce than either CF or $Fe_2O_3$, showed less reduction conversions than FC67MCS (containing more CF and $Fe_2O_3$), in the same time period, but were comparatively more stable. Figure 8a shows that FC67MCS was able to reach a high conversion initially, but there was a gradual decrease in the rate of reduction and final conversion. The rate of oxidation in FC67MCS also decreased with cycle number. In contrast, both FC67(MCS,36h) and FC67(COP,12h) were always able to fully and rapidly re-oxidise (Figure 8d & f). For the reduction steps, FC67(MCS,36h) and FC67(COP,12h) appeared to become more reactive upon cycling (Figure 8c & e) but did not reach the final conversion achieved by FC67MCS, which was calcined for only 6 hours.

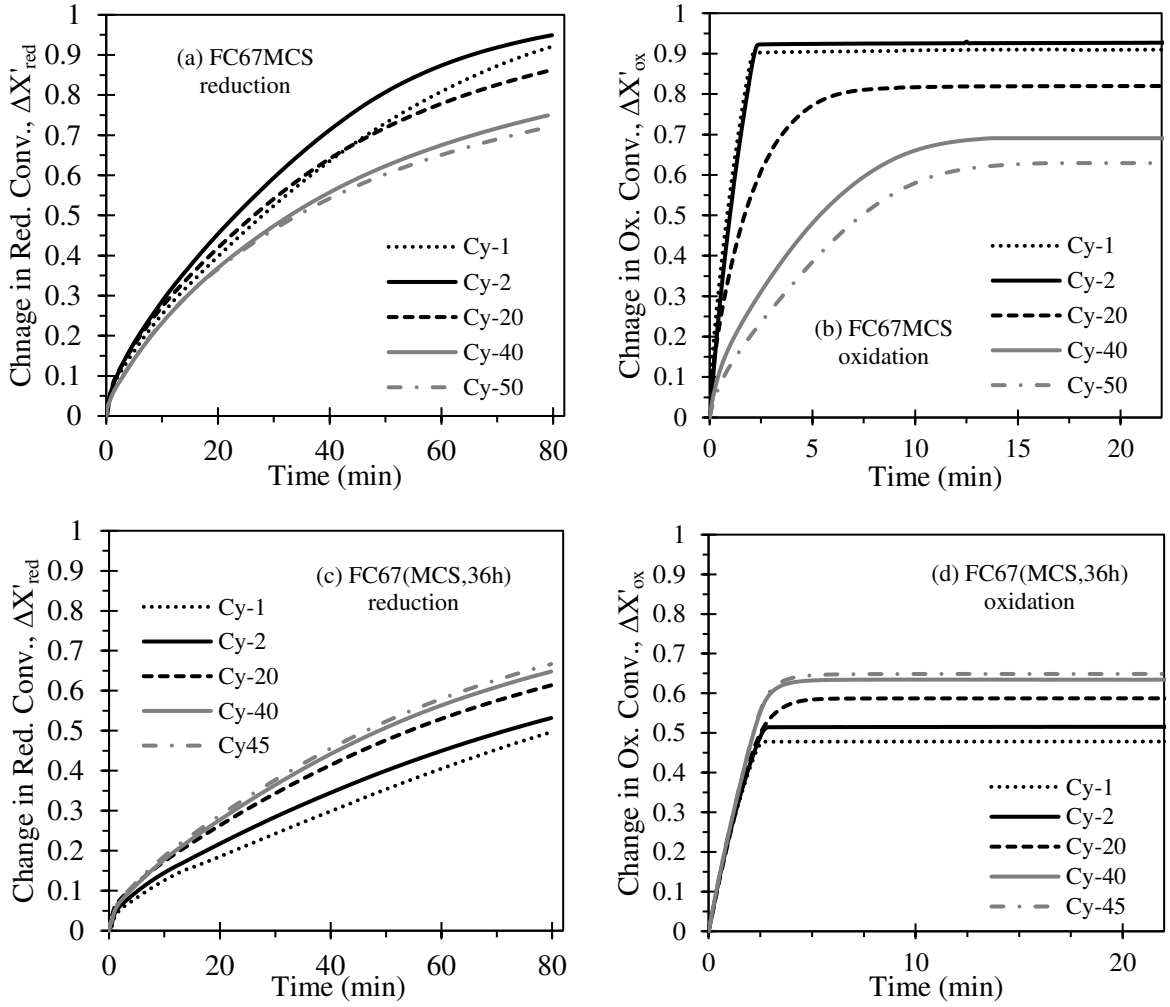

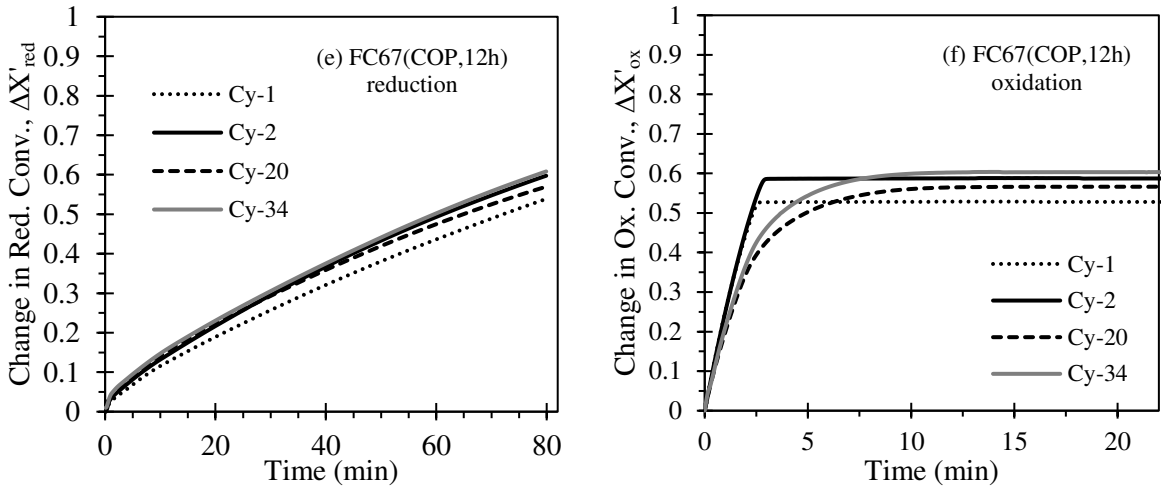


*Figure 8: Change in conversion with time during redox cycling at the specified cycle number in a TGA at 900 °C. The samples were reduced for 80 mins using 5 vol.% $H_2$ and oxidised for 40 min using air. (a) Reduction and (b) oxidation of FC67MCS. (c) Reduction and (d) oxidation of FC67(MCS,36h). (e) Reduction and (f) oxidation of FC67(COP,6h). Only the first 20 mins of the oxidation stages (in b, d and f) are shown for clarity.*

### 4.5 Effect of Temperature in Redox Cycles

Figure 9 shows the mass of the FC67(MCS,36h) particles during two cycles of reduction and oxidation in the TGA at different temperatures. Here, FC67(MCS,36h) particles were heated (heating rate: 20 °C/min) in air to the specified temperature, followed sequentially by reduction in CO for 3 h, partial oxidation in $CO_2$ for 2 h and a final oxidation in air for 30 mins.

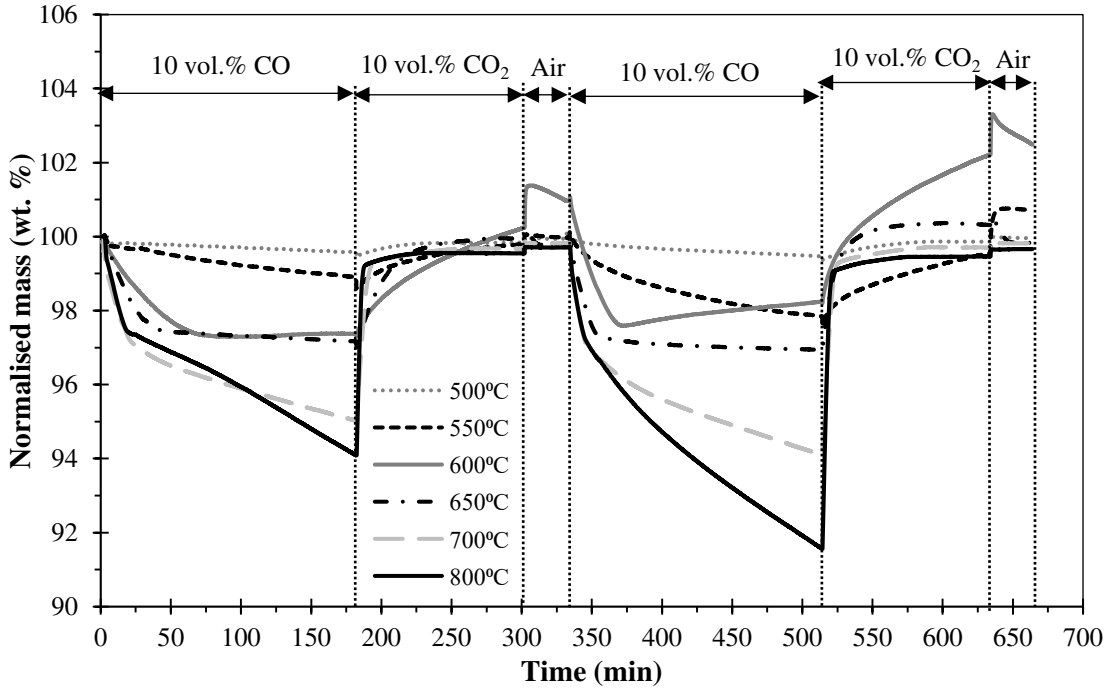


*Figure 9: Normalised mass of FC67(MCS,36h) during reduction with CO for 3 h and oxidation with $CO_2$ for 2 h followed by oxidation with air for 30 min at different isothermal conditions.*

As can be seen from Figure 9, with an increase of temperature, both the rate of reduction and the overall mass loss during reduction were found to increase. When the particles were reduced at 500 – 650 °C and then oxidised at the same temperature with $CO_2$, carbonation of the materials occurred, indicated by the mass of the sample exceeding the initial mass by up to 3.2%. This excess mass was then partially removed as the sample calcined during oxidation with air.

An additional set of experiments was performed to examine the effect of temperature on the relative rates of carbonation and oxidation in $CO_2$ of the reduced sample. Figure 10 shows the results of these experiments, where a sample of FC67(MCS,36h) was first subjected to a sequence of reduction, oxidation and then reduction at 900 °C. The sample was then held isothermally at a different temperature between 400 – 900 °C whilst it was oxidised by $CO_2$ and then air. Difficulties with the gas-switching valves led to the experiments at 500 °C and 600 °C having a slightly longer oxidation in $CO_2$ before the final oxidation in air. The gain in mass during the oxidation with $CO_2$ was due to the carbonation of calcium-containing phases and, or, from the oxidation of iron-rich impurity phases. In the absence of both carbonation and the interaction between the iron- and calcium-containing phases, $CO_2$ would only be able to oxidise iron to magnetite, leading to a final mass of 98.04% (marked on Figure 10).

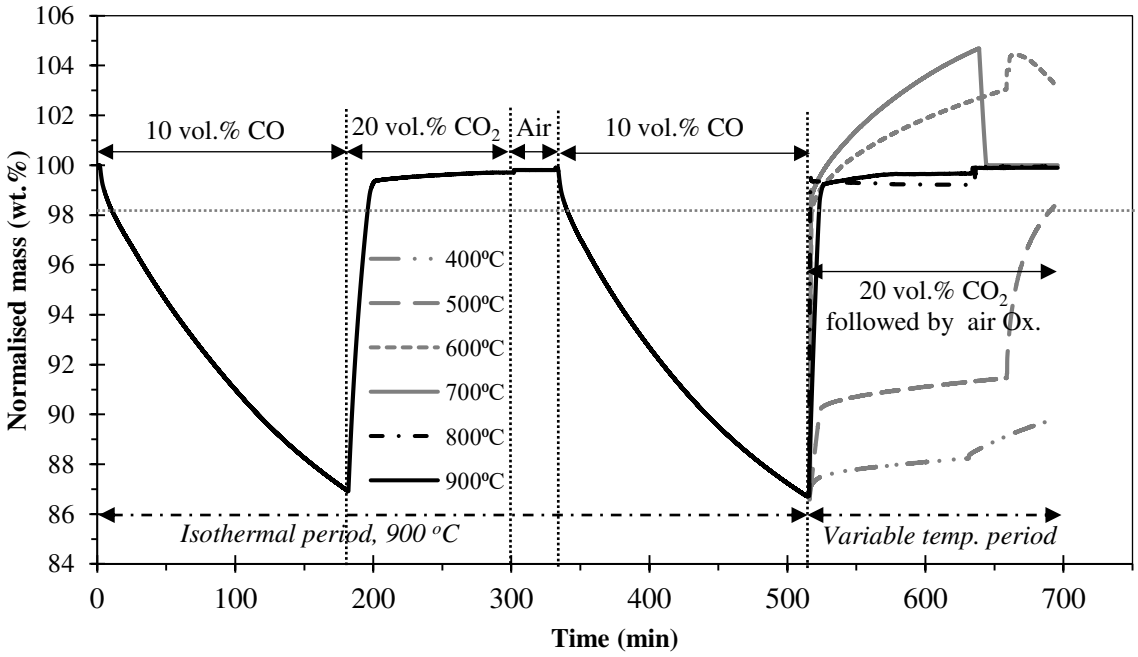


*Figure 10: Effect of oxidation temperature on the extent of carbonation of FC67(MCS,36h) during cycling. The sample, at 900 °C, was reduced in 10 vol% CO, oxidised in 20 vol% $CO_2$ and then in air, and reduced in 10% CO at 900 °C before being oxidised at different temperatures isothermally. The horizontal dotted line indicates the expected mass if the iron is in an oxidation state equivalent to $Fe_3O_4$.*

Upon re-oxidation with $CO_2$ in the second cycle at the different specified temperature, there was an initial rapid gain in mass followed by a slower gain in mass. At 400 $^oC$ and 500 $^oC$, it was difficult to differentiate between carbonation and oxidation; the reaction was not particularly fast and only 36.1% of the mass lost during reduction was recovered by 2 h of oxidation with 20 vol% $CO_2$ at 500 $^oC$. At 600 $^oC$ and 700 $^oC$, carbonation can probably be ascribed to the second, slower reaction stage, which allowed the mass to increase beyond the initial sample mass. Therefore, the reduced particles showed carbonation during $CO_2$ oxidation at temperatures between 600 $^oC$ and 700 $^oC$; with the rate of carbonation being the highest at 700 $^oC$. The initial rapid gain in mass, although most likely to be due to oxidation, may have had some contribution from carbonation. At 600 $^oC$ and 700 $^oC$, the oxidation in air caused the material to decarbonate in addition to completing the oxidation, which lead to the recovery of the starting mass.

On the other hand, 94.2 wt% and 97.5 wt% of the mass lost during reduction was recovered by oxidation in $CO_2$ at 800 $^oC$ and 900 $^oC$, which was consistent with the thermodynamics that suggests phases of CaO and Fe should be able to regenerate $C_2F$ with $CO_2$ or steam as the oxidant. Additionally, there was no evidence of carbonation at these temperatures. Free CaO, which should have been formed on reduction, was not able to carbonate (owing to mixing with the purge gas in the TGA which diluted the 20% $CO_2$ down to ~10%, confirmed by a calibration with a sample of pure CaO by a nominal feed of 20 vol% $CO_2$). Whilst the rapid gain in mass during oxidation was still in excess of the hypothetical change in mass if the iron content were to be converted to an oxidation state equivalent to magnetite; the incomplete regeneration indicates the presence of impurity phases that would only reoxidise in air.

### 4.6 Carbonation Behaviour of Fresh FC67 ($C_2F$) Materials

Figure 2 showed that $C_2F$ can form $CaCO_3$ at ≤ 437 $^oC$ in 20 vol% $CO_2$ and at ≤ 498 $^oC$ in 100 vol% $CO_2$. Figure 11 shows the conversion of the calcium oxide to carbonate (*i.e.* moles of $CO_2$ absorbed/ total theoretical capacity for $CO_2$ absorption) when 100% $CO_2$ was fed to the TGA. An experiment using pure CaO served as a rough calibration (not shown here), and was observed to decompose at a temperature of ~ 842 $^oC$, which, with reference to Figure 2, shows that the concentration of $CO_2$ in contact with the sample is approximately 50 vol% (due to mixing with the protective and purge gases). Under the same experimental conditions, $C_2F$ was expected to carbonate or decarbonate at around 463 $^oC$. Any CF in the particles would be able (thermodynamically) to carbonate below ~ 600 $^oC$.

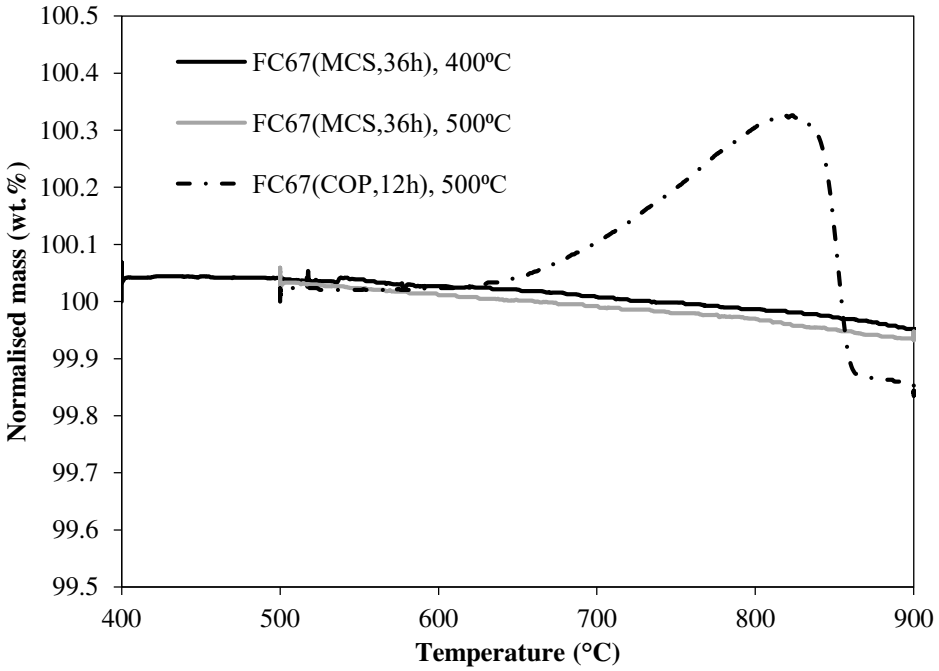


*Figure 11: The extent of carbonation of fresh FC67 and CaO using 100 vol.% $CO_2$, as a function of temperature. Before start of the carbonation experiments, the materials were calcined at 900 °C for 10 min in air, and cooled to room temperature to ensure that there was no carbonate in the fresh materials. The particles were then exposed to a constant temperature of either 400 °C or 500 °C in 100 vol.% $CO_2$ for one hour, followed by a temperature ramp (5 °C/min) to 900 °C using 100 vol.% $CO_2$ to identify the decomposition temperature of any carbonates formed during the isothermal period.*

It is clear that the uptake of $CO_2$ in $C_2F$ was small, much less than that expected from its CaO content, which indicates that its carbonation is kinetically slow[37,38]. This is apparent from the small conversions observed at temperatures (≤ 463 ºC) where carbonation would be expected. Only FC67(COP,12h) showed any detectable carbonation (a virtually negligible gain in mass of 0.3 wt%). This sample contained free CaO impurities, which probably carbonated more readily. Furthermore, no evidence of free $Fe_2O_3$ or $CaCO_3$ was observed in the *ex-situ* XRD analysis of samples of FC67(MCS,36h) and FC67(COP,12h) **(shown in Figure SI7)** recovered by cooling the samples from 900 ºC to ambient temperature in $CO_2$, in the TGA. Thermodynamics suggests carbonation should occur on cooling, however, the fact that the amount of carbonate is below the detection limit of the XRD indicated that the ferrites do not easily carbonate.

### 4.7 Characterisation of the Cycled Particles

Figure 12 shows SEM images of FC67MCS, FC67(MCS,36h) and FC67(COP,12h) after they were either (i) freshly-calcined, (ii) oxidised in air and reduced in CO after ~ 20 cycles in FBR-1 (from the experiments in Figure 5 and Figure 6), or (iii) oxidised in air after up to 50

cycles in TGA (from Figure 8). Fresh FC67MCS (which contains ~ 40 wt.% CF) has a porous structure initially, but visibly degraded over the cycling reactions with some apparent sintering. However, the cross-sectional view after 20 cycles (Figure 12c) showed that it maintained a porous structure in the core and little evidence of sintering was observed. The surface of FC67(MCS,36h) maintained its porosity after 20 cycles in fluidised bed, with negligible sintering (Figure 12e). However, after 50 cycles in TGA, there was some agglomeration with a loss of porosity as seen in Figure 12g. The image of freshly calcined FC67(COP,12h) showed relatively larger grains (Figure 12h). After cycling experiments, a mixture of large and small pores, with a degree of sintering, were observed (Figure 12i), indicating the growth of grains.

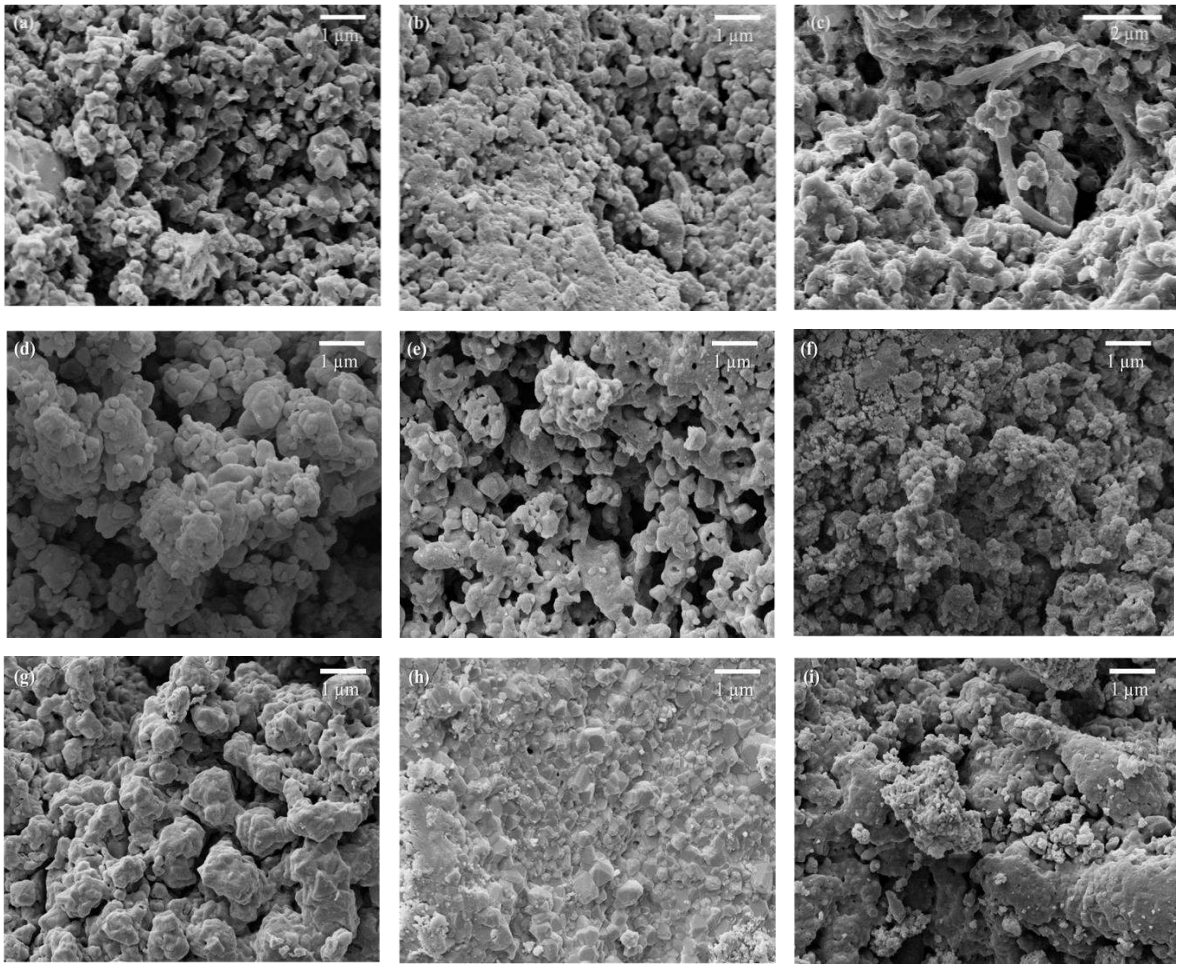


*Figure 12: SEM images of FC67 samples under various conditions. (a - c) FC67MCS after oxidation in air, with (a) the surface of a freshly calcined sample, (b) and (c), the surface and cross-section, respectively, after 20 cycles at 900 °C in FBR-1. (d - g) Surfaces of FC67(MCS,36h), with (d) a freshly calcined sample, (e) and (f), air-oxidised and CO-reduced samples, respectively, after 22 cycles at 900 °C in FBR-1 and (g) an air-oxidised sample after 50 cycles at 900 °C in TGA. (h - i) Surfaces of FC67(COP,16h), with (h) a freshly calcined sample and (i) an air-oxidised sample after 20 cycles at 900 °C in FBR-1.*

The XRD patterns of the cycled materials (recovered after oxidation in air) obtained from FBR-1 are shown in Figure 13. Here, only the unique peaks of $Fe_2O_3$, $CaFe_2O_4$ and CaO are marked. The unmarked peaks are mostly $C_2F$ with a few overlapping peaks of $Fe_2O_3$ and CF. The presence of free $Fe_2O_3$ and CaO in the cycled particles of FC67MCS indicates that segregation occurred over cycling. In contrast, no evidence of free $Fe_2O_3$ was observed in FC67(MCS,36h) or FC67(COP,12h) after 20 cycles. The CaO peaks in the cycled FC67(COP,12h) was attributed to the pre-existing free CaO in the fresh material **(shown in Figure SI2)**. The results suggest that $C_2F$ was relatively stable over the cycling reactions and that it was mostly the impure phases (mostly $CaFe_2O_4$) which segregated.

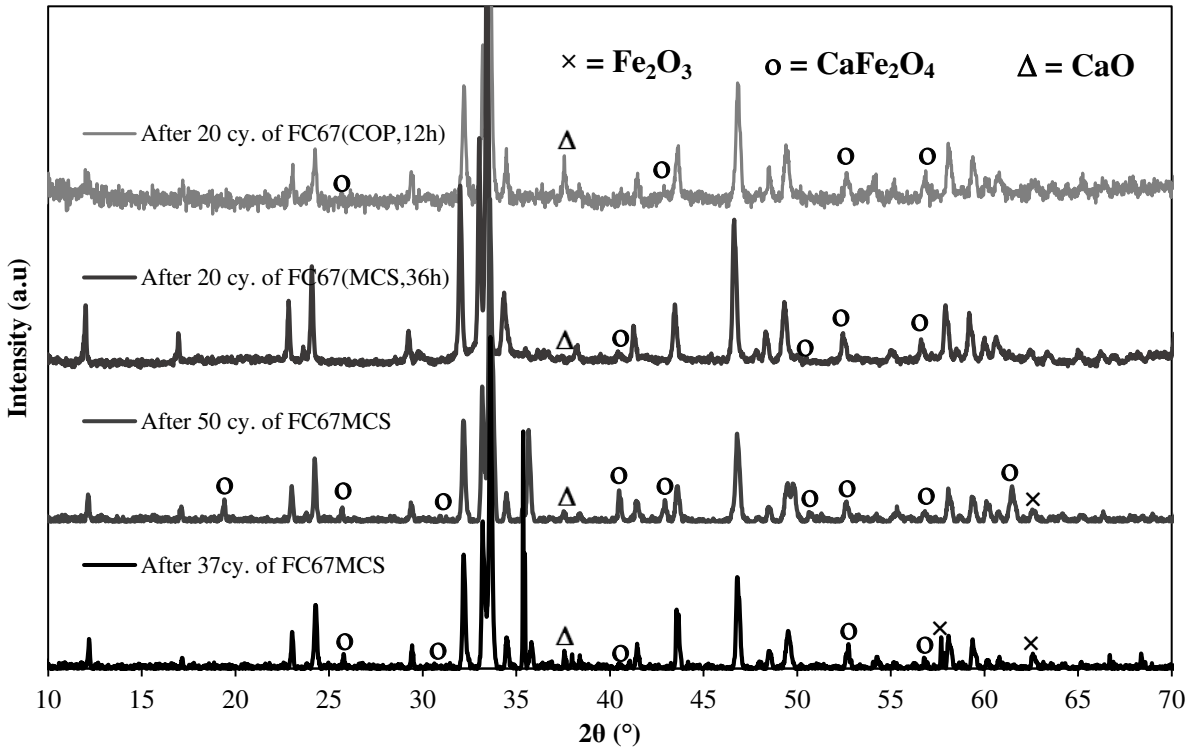


*Figure 13: XRD patterns of FBR cycled air oxidised form FC67 oxygen carriers. The cycling experiments were performed in FBR-1 at 900°C as stated in Figure 5 and Figure 6. The unique peaks of $Fe_2O_3$, $CaFe_2O_4$ and CaO peaks are labelled by '×', 'o' and 'Δ, respectively.*

The measured BET surface areas for these materials (**shown in Table SI2)** were very low (~ 1 $m^2/g$), indicating very little micro-porosity. The surface area of the unsupported $Fe_2O_3$ (FC0) decreased rapidly, losing most of its surface area after 10 cycles. In contrast, for FC67MCS, there was only a 29 % loss in its specific surface area even after the 50 cycles in the fluidised bed experiments. The fresh materials containing higher amounts of $C_2F$, *viz.* FC67(MCS,36h) and FC67(COP,12h), had a low surface area and pore volume initially but this apparently increased (though still to a low value) over the cycling experiments. Among the FC67

materials, fresh particles prepared by COP methods had the lowest surface area (~ 0.5 $m^2/g$). In contrast, the surface area of materials containing comparatively more CF (FC67MCS) decreased more rapidly than the other samples with cycling. The samples which had the highest content of $C_2F$ were produced using more severe calcination conditions (*e.g.* 36 h compared to 6 h for the MCS sample), which tend to destroy porosity. Hence, it is difficult to link the initial pore structure purely to the amounts of different phases present from the current results. No evidence of agglomeration was observed in any of the recovered FC67 materials except for FC67MCS after the fluidised bed experiments. A total of 2 - 4 wt.% loss of sample occurred due to attrition during redox cycles with the particles prepared by the MCS method. The overall attrition was higher in the case of particles synthesised by COP method (~ 3 - 5.5 wt.%). It is believed that the particles were blown out from the reactor as dust (Confirmed by measuring the mass change of sample before and after the experiment and the deposition of dust inside the drying tube was found).

## 5. Discussions

Addition of 66.7 mol.% of CaO to $Fe_2O_3$ decreases the specific oxygen carrying capacity (*i.e.* transferrable oxygen per gram of carrier) and makes the oxygen less available for chemical looping combustion because of the shift in its oxidising potential. The reduction of $C_2F$ occurs at much lower equivalent partial pressures of oxygen than the conditions typically used in CLC. This also means that the equilibrium value of $P_{H_2}/P_{H_2O}$ for the oxidation of metallic iron to $C_2F$ is higher than that for iron to wüstite, so that less steam is required to produce the same amount of hydrogen. Thus, $C_2F$ alone is not suitable for chemical looping combustion but is more suited for the production of hydrogen. Thus, a process which aim is to produce both $H_2$ and pure $CO_2$ would require the material to be used in conjunction with other oxygen carriers with which have phase transitions suitable for combustion.[47] This would require multiple reactors if well mixed, or unmixed systems such as packed beds operating in various configurations.[47]

**Figure SI3** and **Figure SI5** show the presence of small amounts of impurities ($Fe_2O_3$, CF, CaO *etc.*) along with the target phase ($C_2F$) in the fresh oxygen carriers; indicated by several stages of reduction in the TPR, rather than a single stage corresponding to a single phase transition expected for pure $C_2F$. The oxygen carrier prepared by COP method was close to pure $C_2F$, whereas those produced by MCS method gave a mixture of CF and $C_2F$ **(Table SI1).** This indicates that COP method gives better dispersion of the precursors and promotes better interaction between the components. In the cycling experiments, when pure $Fe_2O_3$ was

deeply reduced to mostly iron, it deactivated quickly and resulted in severe sintering. In contrast, all FC67 particles were stable over many more cycles than unmodified iron oxide, even when they were reduced deeply. Very deep reduction of the FC67MCS material, as seen in the TGA experiments (Figure 8a & b), did result in noticeable deactivation, reflected by the decrease in the apparent rates of reduction and oxidation. The larger amount of CF (~ 40 wt.%) in FC67MCS made it easier to reduce, meaning that in a fixed time, this material was able to reduce more deeply, producing more Fe, and making it more susceptible to deactivation. The particles containing a higher amount of $C_2F$ (*e.g.* FC67(COP,12h)) underwent reduction to a lesser extent (up to 66% conversion on reduction) in the specified time in TGA, and showed less change in reactivity over the course of cycling. This contrasts with the results of the fluidised bed experiments in Figure 5 in which each of the FC67 materials initially had a high conversion. In general, the particles which contained the most impurities (FC67MCS) deactivated the most, and the materials with a higher purity of $C_2F$ showed little deactivation. It is difficult to say why the material containing the most $C_2F$ exhibits less deactivation. Deactivation in the pure metal oxide is likely be caused by sintering leading to large grains, a lower porosity and a slow-down in kinetics, such that kinetics becomes limited by the rate of diffusion through product layers. The reformation of the $C_2F$ phase (in which the CaO incorporated back into the phase) during re-oxidation and the precipitation of CaO phase from it as it reduces may help to maintain porosity. When the iron and calcium were segregated, either initially or because of cycling, it is likely that large regions of the particle may have behaved as pure iron oxide, unable to interact with the calcium and deactivating locally as for the pure iron oxide.

Large differences in the rate of reduction were seen between the experiments in the fluidised bed and in the TGA. In the TGA experiments (Figure 9 and Figure 10), the reduction of FC67(MCS,36h) using 10 % CO did not complete even after 180 minutes. In contrast, for the fluidised bed experiments (Figure 5), 95% reduction was achieved after only 13 mins of reduction in 10 vol% CO. Whilst there was some dilution of the gases within the TGA, (~ 50% dilution based on the carbonation experiments), it does not account for the order of magnitude difference in the rates. The products of the reaction, $CO_2$ and $H_2O$, have a large effect on the rate of reduction because of the low equilibrium values of $\frac{P_{CO_2}}{P_{CO}}$ and $\frac{P_{H_2O}}{P_{H_2}}$ associated with $Ca_2Fe_2O_5 \rightleftharpoons 2Fe + 2CaO + 1.5O_2$; only a small amount of either $CO_2$ or $H_2O$ is sufficient to suppress the reduction of $Ca_2Fe_2O_5$. In the TGA, during re-oxidation with $CO_2$, the rate was fast (see Figure 10), and probably influenced by the mass transfer of reactant to the sample.

During reduction, the rate was less likely to be limited by the rate of reactant diffusing to the sample, since the rate of reduction was much slower than oxidation. However, $CO_2$ must be removed from near the surface of the sample, and even a small build-up of $CO_2$ was sufficient to alter the rates of reduction. In the fluidised bed, the rates of mass transfer were much higher, and the particles were better dispersed, so it was less likely that mass transfer of $CO_2$ away from the particles limited the rate.

Both the CF and $C_2F$ were able to regenerate during oxidation, despite the formation of small amounts of free $Fe_2O_3$ and CaO. Particles that contain mostly $C_2F$ (*e.g.* FC67(COP,12h)) did not show any phase segregation even after 20 cycles in the FBR (Figure 13). Previous work on samples containing large amounts of CF have shown that this phase segregated over the course of redox cycles,[44,60] suggesting that most of the segregation observed comes from the presence of impurities such as CF initially in the particles, as is the case for FC67MCS.

### 5.1 $C_2F$ Regeneration and Carbonation

The phase diagram presented in Figure 2 shows that pure $C_2F$ could be carbonated with 100 vol% $CO_2$ at ≤ 498 ºC (or with 50 vol% $CO_2$ at ≤ 463 ºC). However, here the freshly calcined FC67 samples showed no or negligible (if the particles contained some free CaO) carbonation at this temperature (Figure 11), indicating the carbonation reaction has slow kinetics at this temperature. Figure 1 shows that CaO + Fe can be easily re-oxidised to $C_2F$. Here, re-oxidation of FC67(MCS,36h) by air, reduced in prior TPR experiments, was found to be very fast, completing in ~ 300 s **(shown in Figure SI6a & b)**. Furthermore, experimental results (Figure SI6b and Figure 10) suggest that reduced samples of FC67(MCS,36h) and FC67(COP,12h) can almost be completely recovered their original mass during re-oxidation with $CO_2$, with only a small fraction oxidisable only by air. The gain in mass during oxidation with $CO_2$ of the reduced FC67(MCS,36h) matched well with that of expected if all of the iron originally held within the $C_2F$ phase were to be oxidised back to $C_2F$, and if the iron initially within the CF phase were to be oxidised to a phase equivalent to the oxidation state of magnetite. In the case of FC67(COP,12h), which contains ~ 97 wt.% $C_2F$ (**composition shown in Table SI1**), the incomplete oxidation with $CO_2$ may be due to the presence of some free CaO (~ 3 wt.% in the fresh material) or deactivation of the OCs during the redox process. These observations, along with the XRD patterns of particles oxidised in $CO_2$ **(shown in Figure SI7),** suggest that $C_2F$, when reduced, gives well dispersed phases of CaO and Fe, which regenerate readily to $C_2F$ when oxidised with $CO_2$ (or steam). The equilibrium conversion of the gases during the oxidation stage is controlled by the reaction:

$$2Fe + 2CaO + 3H_2O \rightleftharpoons 3H_2 + Ca_2Fe_2O_5 \quad (7)$$

This would achieve a higher conversion of steam than the oxidation of chemically unmodified iron to magnetite.

The experimental results shown in section 4.5 indicate that a temperature higher than 700 $^oC$ is required to avoid carbonation during redox cycling. In order to prevent carbonation at a given partial pressure of $CO_2$, the temperature has to be above the equilibrium temperature for pure CaO, not merely $C_2F$, because the product of reduction, CaO, can carbonate more readily.

## 6. Conclusions

Mechanochemical synthesis and co-precipitation were used for the synthesis of $Ca_2Fe_2O_5$ oxygen carriers. The freshly prepared materials contained mainly $Ca_2Fe_2O_5$ with small amounts of $CaFe_2O_4$ and free CaO. The materials containing a higher purity of $Ca_2Fe_2O_5$ showed a more stable performance over cycles of oxidation and reduction, and similar results were obtained when $CO_2$ was used as the oxidant in place of steam.

Thermodynamics suggest that the regeneration of $Ca_2Fe_2O_5$ in steam would give a higher conversion of steam to hydrogen, as well as a higher hydrogen-producing capacity (per mole of iron) compared to unmodified iron oxide. However, this also means that during reduction, complete combustion of the fuel would not be possible, *i.e.* an oxygen carrier composed of pure $Ca_2Fe_2O_5$ would not be suitable for chemical looping combustion. When reduced $Ca_2Fe_2O_5$ was oxidised in $CO_2$ (analogous to oxidation in steam), it was nearly completely oxidised. This indicated that $Ca_2Fe_2O_5$ can form quickly when phases of calcium oxide and iron are well dispersed, so that the observed equilibrium is for $2Fe + 2CaO + 3CO_2 \rightleftharpoons 3CO + Ca_2Fe_2O_5$.

Oxidised $Ca_2Fe_2O_5$ did not carbonate in ~ 50 vol% $CO_2$, 1 atm even at 400°C, despite being thermodynamically feasible, suggesting that carbonation is severely limited by kinetics. Samples containing the mono-calcium ferrite carbonated but only to a limited extent. However, between 500 – 700 $^oC$, re-oxidation of the reduced samples (of pure $Ca_2Fe_2O_5$), which contained free CaO, resulted in carbonation, but not at higher temperatures. Thus, carbonation can be avoided entirely by operating at temperatures above the carbonation temperature for CaO.

## 7. Acknowledgements

The authors would like to thank Prof. Clare Grey for access to the XRD diffractometer and Z. Saracevic for support in operating the gas adsorption analyser. This work was supported by the

Engineering and Physical Sciences Research Council (EPSRC grants EP/I070912/1 and EP/K030132/1). The first author is grateful to IDB (Islamic Development Bank) - Cambridge International Scholarship body for financial support for PhD study. M.S.C.C acknowledges financial support from an EPSRC Doctoral Training Grant. M.T.D acknowledges funding from the Cambridge Trusts and Trinity College, Cambridge.

## 8. Data

All the supporting data for this work can be found on https://www.repository.cam.ac.uk

## 9. References

(1) IEA. *$CO_2$ Emissions from Fuel Combustion: Highlights*; 2012.

(2) Holloway, S. *Phil. Trans. R. Soc. A* **2007**, *365*, 1095–1107.

(3) IPCC. *Climate Change 2007: Mitigation: Contribution of Working Group III to the Fourth Assessment Report of the Intergovernmental Panel on Climate Change: Summary for Policymakers and Technical Summary*; Metz, B., Davidson, O., Bosch, P., Dave, R., Meyer, L., Eds.; Cambridge University Press, 2007.

(4) Jin, H.; Ishida, M. *Fuel* **2004**, *83* (17-18), 2411–2417.

(5) Leion, H.; Mattisson, T.; Lyngfelt, A. *Energy Fuel* **2009**, *23*, 2307–2315.

(6) Bohn, C. D.; Müller, C. R.; Cleeton, J. P.; Hayhurst, A. N.; Davidson, J. F.; Scott, S. A.; Dennis, J. S. *Ind. Eng. Chem. Res.* **2008**, *47*, 7623–7630.

(7) Aston, V. J.; Evanko, B. W.; Weimer, A. W. *Int. J. Hydrogen Energy* **2013**, *38* (22), 9085–9096.

(8) Scheffe, J. R.; Allendorf, M. D.; Coker, E. N.; Jacobs, B. W.; Mcdaniel, A. H.; Weimer, A. W. *Chem. Mater.* **2011**, *23*, 2030–2038.

(9) Messerschmitt, A. Process of producing hydrogen.- U.S. Patent No. 971,206. U.S. Patent No. 971,206, 1910.

(10) Fan, L.-S.; Zeng, L.; Wang, W.; Luo, S. *Energy Environ. Sci.* **2012**, *5* (6), 7254.

(11) Chiesa, P.; Lozza, G.; Malandrino, A.; Romano, M.; Piccolo, V. *Int. J. Hydrogen Energy* **2008**, *33* (9), 2233–2245.

(12) Cleeton, J. P. E. Chemical Looping Combustion with Simultaneous Power Generation and Hydrogen Production using Iron Oxides, University of Cambridge, UK, 2011.

(13) He, F.; Li, F. *Energy Environ. Sci.* **2015**, *8* (2), 535–539.

(14) Fan, L.; Li, F. *Ind. Eng. Chem. Res.* **2010**, *49*, 10200–10211.

(15) Kathe, M. V.; Empfield, A.; Na, J.; Blair, E.; Fan, L. S. *Appl. Energy* **2016**, *165*, 183–201.

(16) Adanez, J.; Abad, A.; Garcia-Labiano, F.; Gayan, P.; de Diego, L. F. *Prog. Energy Combust. Sci.* **2012**, *38* (2), 215–282.

(17) Li, F.; Fan, L.-S. *Energy Environ. Sci.* **2008**, *1* (2), 248.

(18) de Diego, L. F.; García-Labiano, F.; Adánez, J.; Gayán, P.; Abad, A.; Corbella, B. M.; Palacios, J. M. *Fuel* **2004**, *83* (13), 1749–1757.

(19) Ishida, M.; Jin, H. *Ind. Eng. Chem. Res* **1996**, *35* (7), 2469–2472.

(20) Johansson, M.; Mattisson, T.; Lyngfelt, A. *Ind. Eng. Chem. Res* **2004**, *43* (22), 6978–6987.

(21) Kierzkowska, A. M.; Bohn, C. D.; Scott, S. A.; Cleeton, J. P.; Dennis, J. S.; Müller, C. R. *Ind. Eng. Chem. Res* **2010**, *49*, 5383–5391.

(22) Kidambi, P. R.; Cleeton, J. P. E.; Scott, S. A.; Dennis, J. S.; Bohn, C. D. *Energy & Fuels* **2012**, *26* (1), 603–617.

(23) Ismail, M.; Liu, W.; Scott, S. A. *Energy Procedia* **2014**, *63*, 87–97.

(24) Adanez, J.; Garcıa-Labiano, F.; de Diego, L. F.; Gayan, P.; Celaya, J.; Abad, A. *Ind. Eng. Chem. Res* **2006**, *45* (8), 2617–2625.

(25) Svoboda, K.; Siewiorek, a.; Baxter, D.; Rogut, J.; Punčochář, M. *Chem. Pap.* **2007**, *61* (2), 110–120.

(26) Song, H.; Doroodchi, E.; Moghtaderi, B. *Energy & Fuels* **2012**, *26*, 75–84.

(27) Liu, W.; Dennis, J. S.; Scott, S. A. *Ind. Eng. Chem. Res.* **2012**, *51*, 16597–16609.

(28) Roux, S.; Bensakhria, A.; G., A.; Antonini, G. *Int. J. Chem. Eng.* **2006**, *4* (1).

(29) Hillert, M.; Selleby, M.; Sundman, B. *Metall. Trans. A* **1990**, *21* (10), 2759–2776.

(30) Lin, H.-T.; Yutai, K.; Josef, M.; Andrew, L. Gyekenyesi & Michael, H. *Ceramic Materials for Energy Applications IV:Ceramic Engineering and Science Proceedings*; John Wiley & Sons, 2015.

(31) Isupova, L. A.; Tsybulya, S. V; Kryukova, G. N.; Budneva, A. A.; Paukshtis, E. A.; Litvak, G. S.; Ivanov, V. P.; Kolomiichuk, V. N.; Pavlyukhin, Y. T.; Sadykov, V. A. *Kinet. Catal.* **2002**, *43* (1), 122–128.

(32) Rao, C. N. R.; Gopalakrishnan, J.; Vidyasagar, K. *Indian J. Chem.* **1984**, *23 A*, 265–284.

(33) Shaula, A. L.; Pivak, Y. V.; Waerenborgh, J. C.; Gaczyñski, P.; Yaremchenko, A. A.; Kharton, V. V. *Solid State Ionics* **2006**, *177* (33-34), 2923–2930.

(34) Hirabayashi, D.; Yoshikawa, T.; Mochizuki, K.; Suzuki, K.; Sakai, Y. *Catal. Letters* **2006**, *110* (3-4), 269–274.

(35) Waerenborgh, J. C.; Figueiredo, F. M.; Frade, J. R.; Colomer, M. T.; Jurado, J. R. *J. Phys. Condens. Matter* **2001**, *13* (35), 8171–8187.

(36) Il'in, A. A. P.; Smirnov, N. N.; Il'in, A. A. P. *Kinet. Catal.* **2006**, *47* (6), 901–906.

(37) Di Felice, L.; Courson, C.; Foscolo, P. U.; Kiennemann, A. *Int. J. Hydrogen Energy* **2011**, *36* (9), 5296–5310.

(38) Huang, B. S.; Chen, H. Y.; Chuang, K. H.; Yang, R. X.; Wey, M. Y. *Int. J. Hydrogen Energy* **2012**, *37* (8), 6511–6518.

(39) Dueso, C.; Thompson, C.; Metcalfe, I. *Appl. Energy* **2015**, *157*, 382–390.

(40) Thursfield, A.; Murugan, A.; Franca, R.; Metcalfe, I. S. *Energy Environ. Sci.* **2012**, *5* (6), 7421–7459.

(41) Khanna, L.; Verma, N. K. *J. Magn. Magn. Mater.* **2013**, *336*, 1–7.

(42) Saleh, H. I. *J. Mater. Sci. Technol.* **2004**, *20* (5), 530–534.

(43) Yin, J.; Lv, X.; Xiang, S.; Bai, C.; Yu, B. *ISIJ Int.* **2013**, *53* (9), 1571–1579.

(44) Ismail, M.; Liu, W.; Dunstan, M. T.; Scott, S. A. *Int. J. Hydrogen Energy* **2016**, *41* (7), 4073–4084.

(45) Jacob, K. T.; Dasgupta, N.; Waseda, Y. *Zeitschrift für Met.* **1999**, *90* (7), 486–490.

(46) Davies, R. H.; Dinsdale, A. T.; Gisby, J. A.; Robinson, J. A. J.; Martin, S. M. *Calphad* **2002**, *26* (2), 229–271.

(47) Chan, M. S. C.; Liu, W.; Ismail, M.; Yang, Y.; Scott, S. A.; Dennis, J. S. *Chem. Eng. J.* **2016**, *296*, 406–411.

(48) Forsberg, S.; Wikstrom, P.; Rosen, E. *Metall. Mater. Trans. B* **2002**, *33* (June), 385–392.

(49) Newman, E. S.; Hoffman, R. *J. Res. Natl. Bur. Stand. (1934).* **1956**, *56* (6), 313.

(50) Turkdogan, E. T.; Fruehan, R. J. In *Steelmaking and Refining*; The AISE Steel Foundation, Pittsburg, PA, 1998; Vol. i, pp 13–157.

(51) Jeon, J.; Jung, S.; Sasaki, Y. *ISIJ Int.* **2010**, *50* (8), 1064–1070.

(52) Donat, F.; Hu, W.; Scott, S. A.; Dennis, J. S. *Ind. Eng. Chem. Res.* **2015**, *54*, 6713 − 6723.

(53) Wen, C.; Yu, Y. *AIChE J.* **2004**, *12* (3), 610–612.

(54) Larson, A. C.; Dreele, R. B. Von. *Los Alamos Natl. Lab. Los Alamos, NM, USA* **1990**.

(55) Toby, B. H. *J. Appl. Crystallogr.* **2001**, *34* (2), 210–213.

(56) Brunauer, S.; Emmett, P.; Teller, E. *J. Am. Chem. Soc.* **1938**, *60* (2), 309–319.

(57) Chuang, S. Y.; Dennis, J. S.; Hayhurst, A. N.; Scott, S. A. *Combust. Flame* **2008**, *154*, 109–121.

(58) Ward, D. A.; Ko, E. I. *Ind. Eng. Chem. Res.* **1995**, *34* (2), 421–433.

(59) Zhou, J. Z.; Xu, Z. P.; Qian, G. In *Nanotechnology for Water and Wastewater*

*Treatment*; Lens, P., Virkutyte, J., Jegatheesan, V., Kim, S. H., Eds.; IWA Publishing, UK, 2013; pp 153–168.

(60) Ismail, M. Development and Evaluation of Iron Oxide-based Oxygen Carriers for Chemical Looping Combustion and Hydrogen Production, University of Cambridge, 2016.

# Supporting Documents

## 1) Temperature Programmed Decomposition (TPD) of the Dried Cake of FC67 Oxygen Carriers

The cake obtained after drying the filtered precipitates (in co-precipitation method) was subjected to a temperature ramp from 100 – 1000 ºC (at a rate of 20 ºC/min, in air) in TGA. The derivatives of mass change as a function of temperature are shown below.

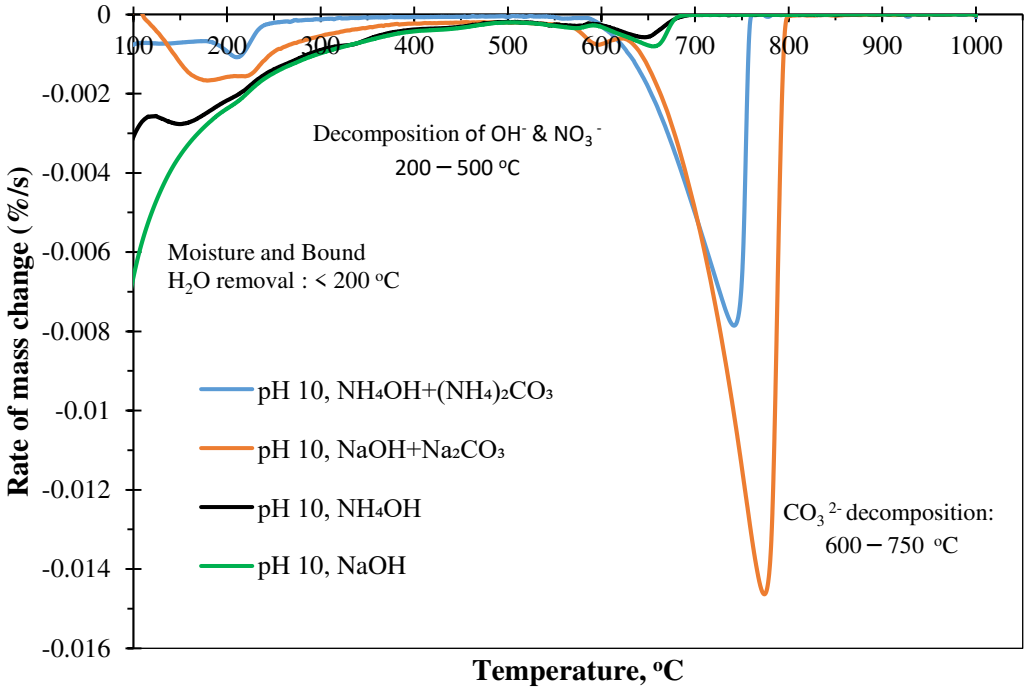


*Figure SI1: Rate of mass change (i.e. DTG) of the TPD at various temperatures during calcination of co-precipitated dried FC67 cake for four of the precipitants, (a) $NH_4OH$ + $(NH_4)_2CO_3$, (b) NaOH + $Na_2CO_3$ (c) $NH_4OH$ and (d) NaOH.*

## 2) XRD Patterns of Co-precipitated Fresh FC67 after Calcination at 1000 °C, 6 h

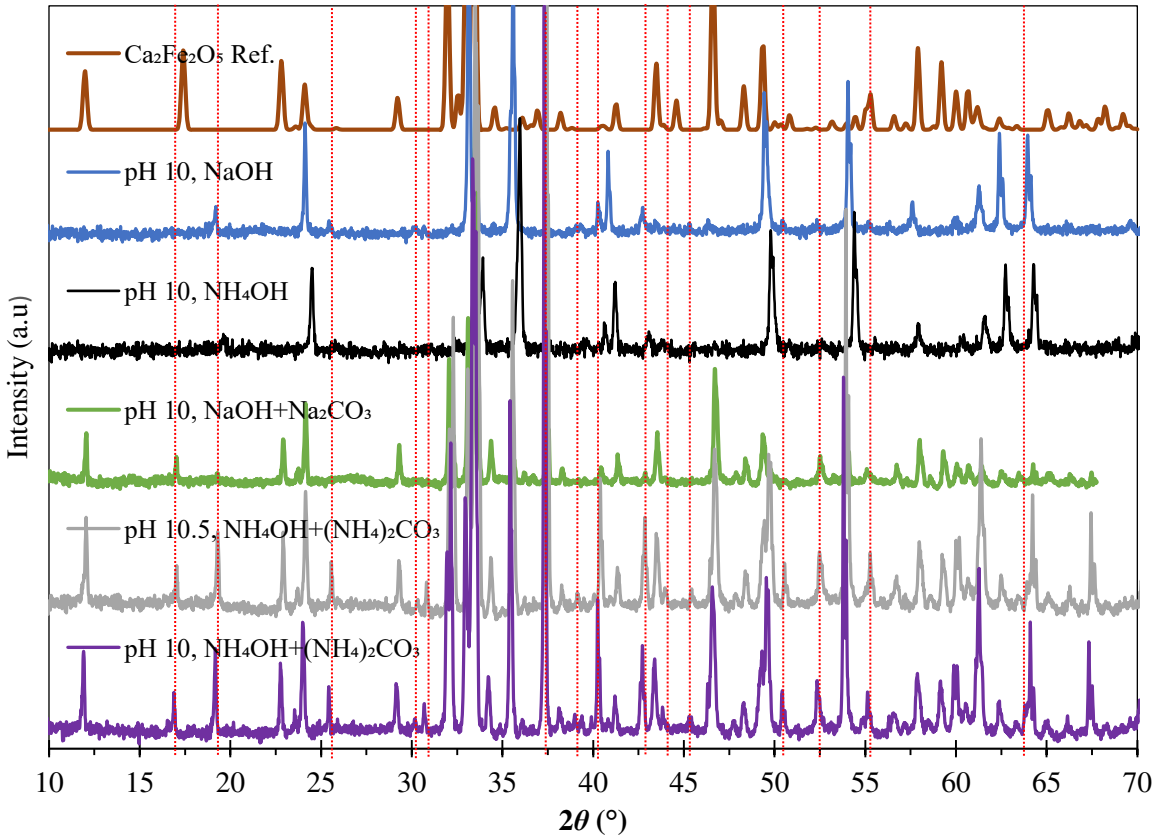


*Figure SI2: XRD patterns of co-precipitated FC67 particles after calcination at 1000 °C for 6 h. Unique (non-overlapping) peaks of $CaFe_2O_4$ are indicated by dotted vertical lines (orange colour).*

### 3) TPR (in $H_2$) of fresh FC67 particles prepared by co-precipitation Method

Figure SI3 shows the TPR (in 5 vol.% $H_2$) and DTG of fresh FC67 particles (calcined at 1000 $^oC$, 6 h) prepared by co-precipitation using different precipitants. The experiments were carried out in TGA. Theoretically, FC67 is expected to lose 17.6% of its mass if it is reduced completely.

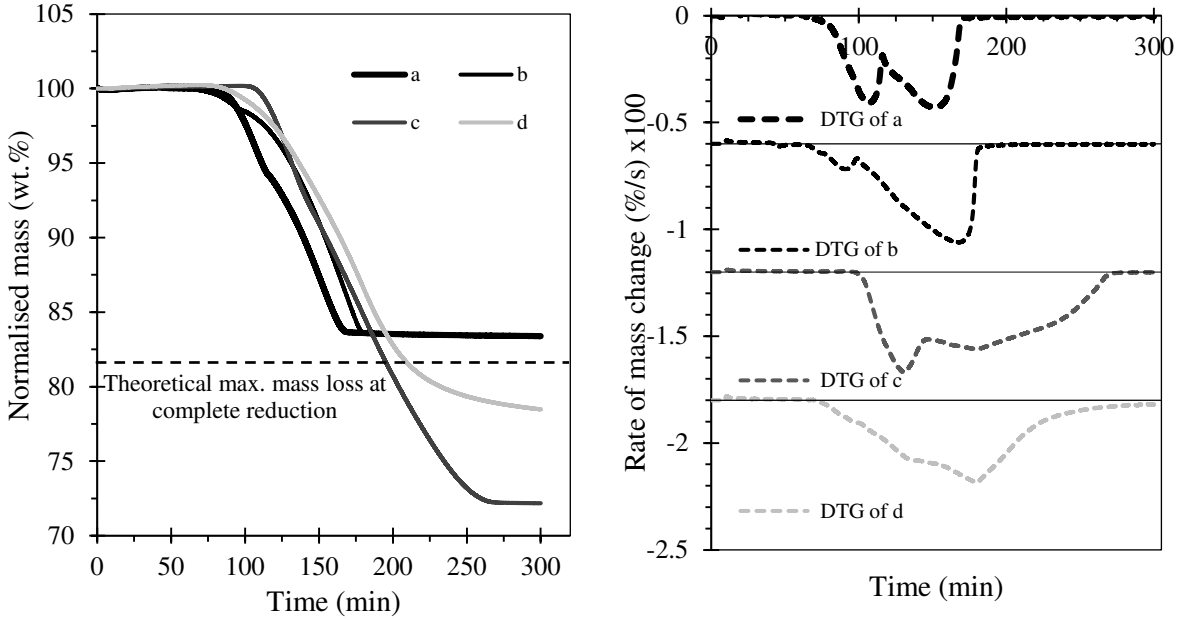


*Figure SI3: Normalised mass duing 5 vol% $H_2$ TPR (Left figure) and DTG (Right figure) of TPR of co-precipitated fresh FC67 particles (calcined at 1000 °C for 6 h. Here: a) OCs prepared by using $NH_4OH$ + $(NH_4)_2CO_3$ with pH-10, b) OCs prepared by using NaOH + $Na_2CO_3$ with pH-10, c) OCs prepared by using $NH_4OH$ with pH-10 and d) OCs prepared by using NaOH with pH-12.5.*

## 4) XRD of the Particles prepared by MCS method

Figure SI4 shows the XRD pattern of the fresh FC67 prepared by MCS method after calcination at 1000 $^{o}$C in air for various durations. At thermodynamic equilibrium, only $C_2F$ should be present after calcination at 1000 $^{o}$C in air. Here, both CF and $C_2F$ were observed even after a 36 h calcination. The characteristic peaks of CaO were also found in the XRD patterns for materials prepared with shorter calcination periods. Unique peaks of CF and CaO are marked by 'O' and '×', respectively. The unmarked peaks are of $C_2F$; it is hard to identify the unique peaks of $Fe_2O_3$ as those are overlapped with either CF or $C_2F$.

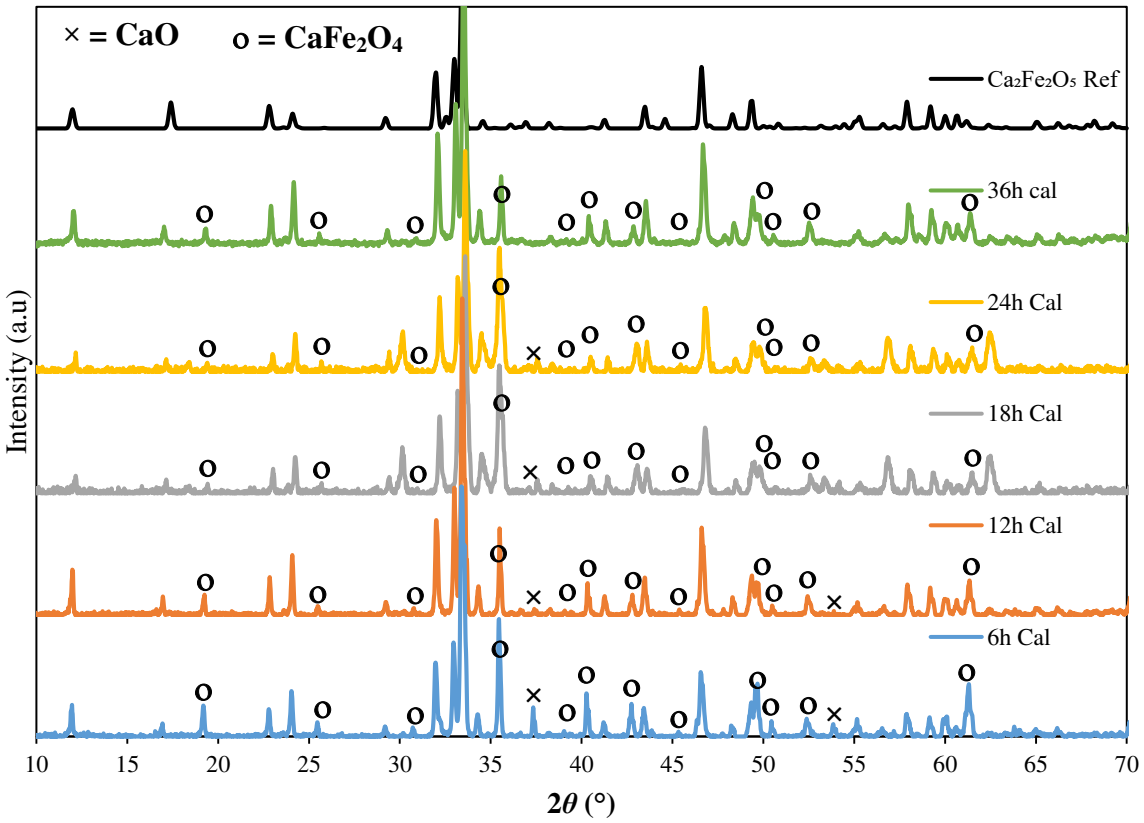


*Figure SI4: XRD patterns of fresh FC67 (prepared by MCS method) calcined at 1000 °C, maintaining different calcination durations. Selected peaks labelled by: O ($CaFe_2O_4$)), × (CaO). The reference XRD patterns used for comparison are: $CaFe_2O_5$ (ICSD- 14296, PCMN), $CaFe_2O_4$ (ICSD- 16695, PNMA) and CaO (ICSD- 51409, FM3-M).*

## 5) TPR (in $H_2$) of fresh FC67 particles prepared by MCS Method

Figure SI5 shows the TPR (in 5 vol.% $H_2$) and DTG of fresh FC67 materials prepared by the MCS method in which the particles were calcined at 1000 °C for different time periods. There is a small difference between the amount of CF in the sample calculated from the first mass loss and the amount determined from XRD (**shown in Table SI1**), possibly owing to reduction of free $Fe_2O_3$ in the particles.

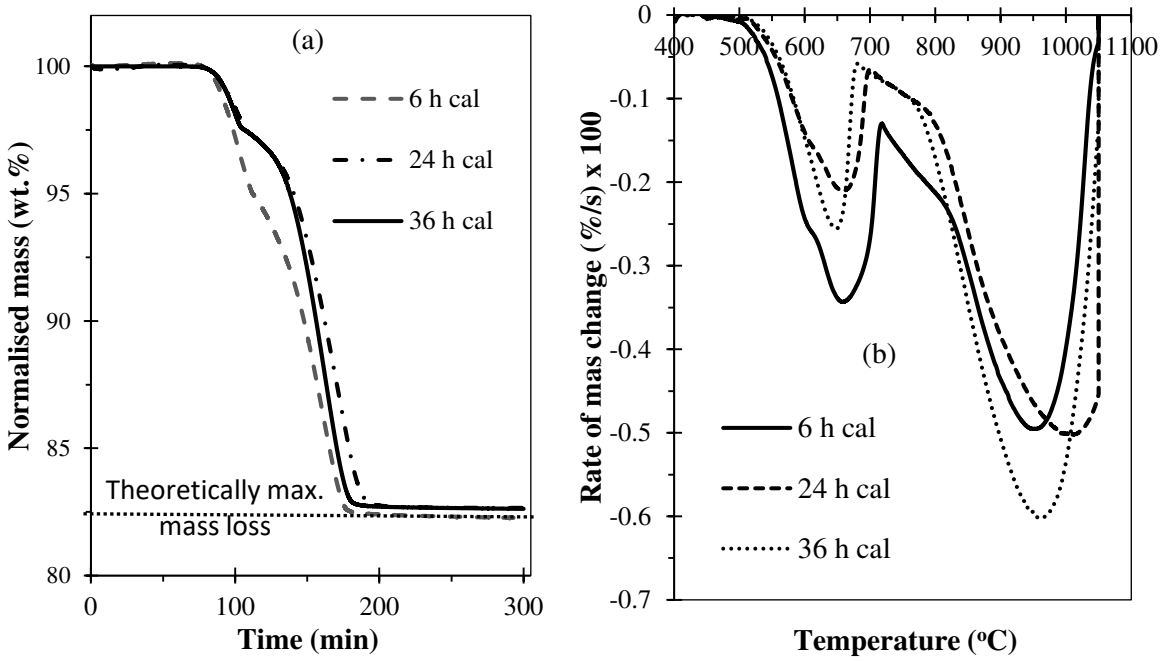


*Figure SI5: (a) Normalised mass change duing TPR in 5 vol% $H_2$ and b) Normalised rate of mass change (with temperature) during TPR of FC67 oxygen carriers prepared by the MCS method in which the particles were calcined at 1000 °C for different time periods.*

## 6) Composition of Phases:

*Table SI1: Composition of phases in the freshly prepared oxygen carriers, quantified by Rietveld refinements of the XRD patterns, and inferred indirectly from the TPR measurements*

| Preparation Method | Calcination temperature | Phase fractions calculated from Rietveld Refinement | | | | | Results from TPR | | |
|---|---|---|---|---|---|---|---|---|---|
| | | $CaFe_2O_4$ (wt. fr.) | $Ca_2Fe_2O_5$ (wt. fr.) | CaO (wt. fr. | $Fe_2O_3$ (wt. fr.) | Total amount of Fe (mol. fr. in OCs | $CaFe_2O_4$ (wt. fr.) based on 1st mass loss during TPR[1] | Temp. (°C) at which 1st mass loss completed | Total amount of Fe (mol. fr.) in OCs |
| Mechanochemical Synthesis | 1000°C, 6h | 0.397 | 0.555 | 0.047 | | 0.53 | 0.46 | 711° C | 0.50 |
| Mechanochemical Synthesis | 1150°C, 6h | 0.294 | 0.704 | 0.008 | | 0.54 | 0.33 | 811 ° C | 0.52 |
| Mechanochemical Synthesis | 1250°C, 6h | Particles melted | | | | | | | |
| Mechanochemical Synthesis | 1150°C,12h | 0.272 | 0.737 | | | 0.54 | 0.29 | 819 ° C | 0.51 |
| Mechanochemical Synthesis | 1000°C, 6h+ 1150°C, 6h | 0.285 | 0.714 | | | 0.54 | 0.29 | 803° C | 0.51 |
| Mechanochemical synthesis | 1000oC, 36h | 0.14 | 0.86 | | | 0.52 | 0.19 | 656° C | 0.49 |
| Mechanochemical Synthesis | 1000°C, 36h + 1150°C, 6h | 0.137 | 0.87 | | | 0.52 | 0.16 | 678° C | 0.49 |
| Co-ppt., pH-10, $(NH_4)_2CO_3 + NH_4OH$ | 1000°C, 6h | 0.22 | 0.672 | 0.11 | - | 0.47 | 0.28 | 722° C | 0.47 |
| (Co-ppt., pH-10, $(NH_4)_2CO_3 + NH_4OH$ | 1150°C, 6h | 0.009 | 0.919 | 0.063 | 0.001 | 0.47 | 0.14 | 705° C | 0.51 |
| Co-ppt., pH-10, $(NH_4)_2CO_3 + NH_4OH$ | 1000°C, 6h + 1150°C, 6h | 0.021 | 0.896 | 0.06 | 0.023 | 0.48 | 0.04 | 697° C | 0.51 |
| Co-ppt., pH-10, $Na_2CO_3 + NaOH$ | 1000°C, 6h | 0.022 | 0.893 | 0.06 | 0.024 | 0.48 | 0.14 | 650° C | 0.47 |
| Co-ppt., pH-10, $Na_2CO_3 + NaOH$ | 1150°C, 6h | 0.003 | 0.924 | 0.057 | 0.016 | 0.48 | 0.03 | 601° C | 0.46 |
| Co-ppt., pH-10, $Na_2CO_3 + NaOH$ | 1000°C, 6h + 1150°C, 6h | - | 0.97 | 0.03 | - | 0.48 | 0.02 | 623° C | 0.47 |

[1]Calculated assuming that only CF and $C_2F$ is present in the particles

## 7) BET surface area, BJH volume and pore size measurements

Table SI2 shows the surface area, BJH volume and average pore size of the fresh and cycled materials.

*Table SI2: Summary of specific surface area, BJH volume and pore width[1] of the freshly prepared particles and particles cycled in the fluidized bed reactor*

| **Particles** | **BET specific surface area ($m^2/g$)** | **BJH volume ($cm^3/g$)** | **'d' pore (nm)** |
|---|---|---|---|
| FC0 fresh | 0.9 | 0.0016 | 8.01 |
| FC67MCS | 1.34 | 0.0024 | 7.03 |
| FC67(MCS,36h) | 1.0 | 0.0022 | 2.4 |
| FC67(COP,12h) | 0.5 | 0.0049 | 6.7 |
| FC0 after 10 cycles | 0.26 | 0.0007 | 9.76 |
| FC67MCS after 10 cycles | 1.36 | 0.0023 | 6.62 |
| FC67MCS after 37 cy | 1.2 | 0.002 | 6.8 |
| FC67MCS after 50 cy | 0.95 | 0.0019 | 5.74 |
| FC67(MCS,36h) after 20 cycles | 1.2 | 0.0025 | 2.97 |
| FC67(COP,12h) after 20 cycles | 1.4 | 0.0476 | 11.68 |

[1]*Adsorption average pore width (4V/A by BET)*

## 8) Temperature Programmed Reduction and Oxidation of Particles

Temperature programmed oxidation (TPO) of FC67(MCS,36h) of the completely reduced sample (*i.e.* after the TPR) was carried out using 20 vol.% $CO_2$. Figure SI6a shows the normalised mass and its derivative as a function of temperature during TPR in $H_2$ and TPO in $CO_2$.

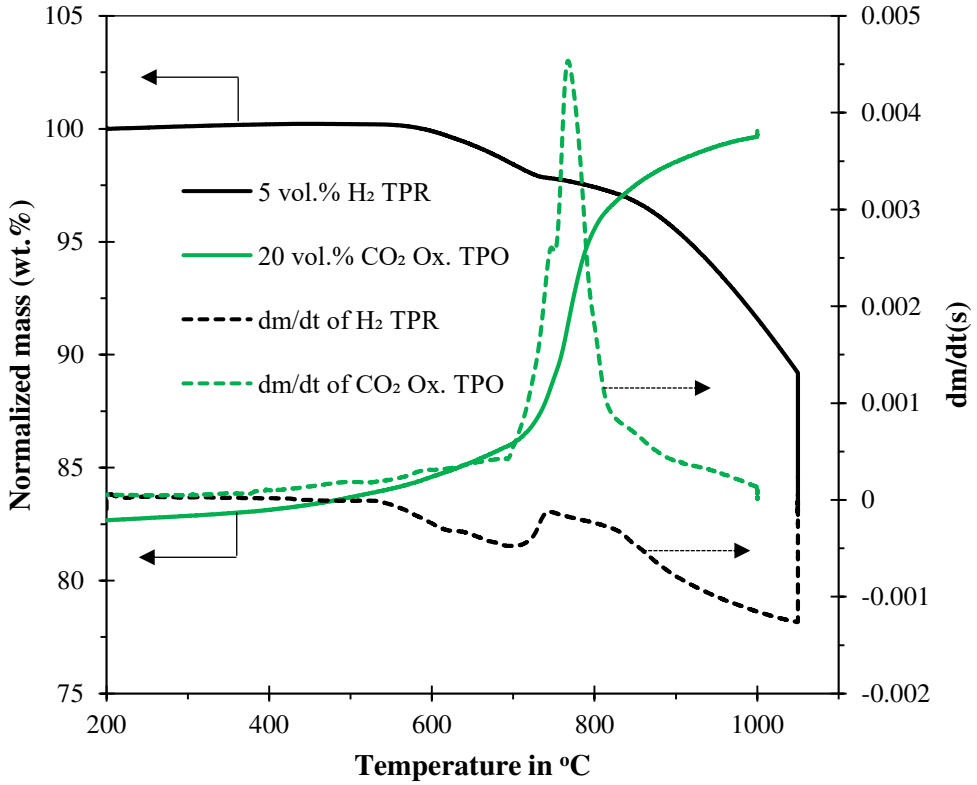


*Figure SI6a: Mass of sample, and its derivative, during $H_2$ TPR followed by $CO_2$ TPO (heating from 50 -1000 °C at a rate of 5 °C/min and then 30 mins at 1000 °C) for fresh FC67(MCS,36h).*

It can be seen that during TPR all the ferrites reduced to Fe and CaO (the mass loss during TPR is consistent with the expected mass loss of 17.7 wt.%). The oxidation (TPO) of the reduced particles by $CO_2$ led to the formation of $CaCO_3$ until ~ 650 °C is reached, when the gradual decomposition of carbonate occurred simultaneously with the oxidation of the iron phases. At temperatures below 650 °C, the oxidation of Fe to FeO or $Fe_3O_4$ or CF or $C_2F$ is kinetically slow [61],[62] and if the oxidation is done by $CO_2$, it may be competitively inhibited by carbonation in the particles. Furthermore, according to **Figure -2**, any free CaO would have been carbonated below 650 °C at $P_{CO_2} = 1$ bar, preventing the formation of Fe-Ca-O phases. During $CO_2$ oxidation of the reduced OCs, ~ 99.7% of the mass lost during TPR was recovered indicating that oxidation of the reduced particles by $CO_2$ could re-generate the $C_2F$ without any need for air oxidation. Additional evidence for this regeneration was also observed during the isothermal $CO_2$ oxidation (at 900 °C) of the reduced (by TPR) particles shown in Figure SI6b. A small fraction (0.3 wt.%) of the lost mass (during reduction) did not fully re-oxidised to a

state equivalent to oxidation of Fe to $Fe_2O_3$ during re-oxidation) during $CO_2$ oxidation at 900 °C (in Figure SI6b) suggests the presence of minor amounts of CF or other iron-containing phases.

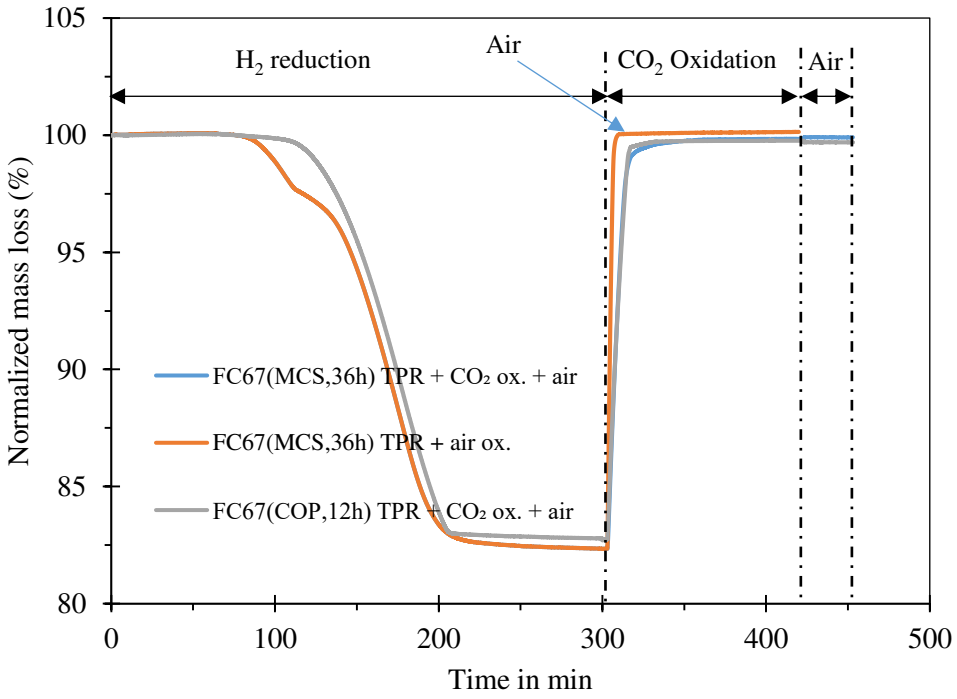


*Figures SI6b: Air oxidation and the $CO_2$ oxidation behaviour* at 900 °C *of TPR reduced particles of FC67(MCS,36h) and FC67(COP,12h).*

## 9) XRD Patterns of the FC67 Particles (Fresh and Reduced) Oxidised by $CO_2$

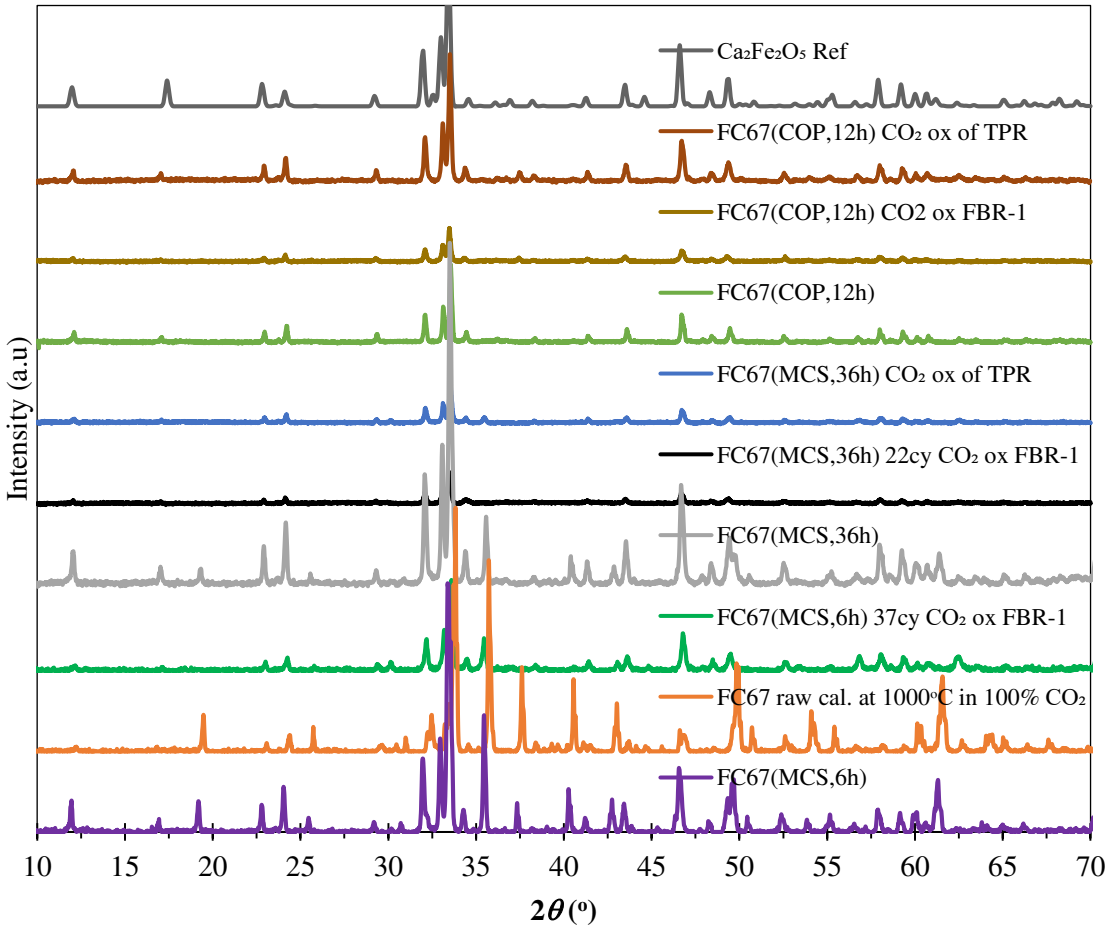


*Figure SI7: XRD of a selection of fresh and $CO_2$ oxidized samples (obtained from FBR-1 and after TPR in TGA). Here, 'FC67 raw Cal. at 1000 °C in 100 % $CO_2$' means the dried (not calcined) particles were calcined at 1000 °C in 100 vol.% $CO_2$ and then XRD of the particle was carried out.*